The effect of intra-molecular bonds on the liquid-liquid critical point in modified-WAC models

E. Lascaris[1]
Department of Chemistry & Physical Sciences, Pace University, New York, NY 10038 USA
(*Electronic mail: elascaris@pace.edu)

(Dated: 2 November 2022)

To obtain a better understanding of liquid-liquid critical points (LLCPs) in one-component liquids, we extend the modified-WAC model by [E. Lascaris, Phys. Rev. Lett. 116, 125701 (2016)] which is known to have a LLCP. The original WAC model is a model for silica (SiO_2) and consists of a mixture of non-bonded Si and O ions. By adding explicit intra-molecular Si-O bonds to the model we are able to study how several parameters (Si-O bond length, O-Si-O angle, and bond stiffness) affect the existence and location of the LLCP. We find that for this model only the Si-O bond length has a strong effect on the LLCP, while the bond angle and bond stiffness have no significant effect on the LLCP. An analysis of the relevant coordination numbers indicates that increasing the bond length decreases the ratio $R_{\mathrm{Si/O}}$ of additional Si ions per additional O ion in the first coordination shell of the Si, which causes the LLCP to move to higher, more accessible temperatures. The behavior of the $R_{\mathrm{Si/O}}$ parameter shows a strong correlation with the behavior of the LLCP and might be a useful tool to determine if a LLCP exists at low, hard-to-reach temperatures in other models.

I. INTRODUCTION

Ever since Poole et al. reported the discovery of a liquid-liquid critical point (LLCP) in the ST2 model of water[1,2], a lot of attention has been given to the question of *is there a LLCP in water?* The existence of a liquid-liquid phase transition (LLPT) that terminates at a LLCP could explain the long list of anomalies that are known to occur in water[3], including the first-order-like phase transition between high-density and low-density amorphous ice seen in experiment[4]. The liquid-liquid critical point hypothesis of water has fueled a heated debate[5–13], which unfortunately eclipsed the more general question of *under what circumstances does a one-component system exhibit a LLPT or LLCP?*

By studying a large variety of models we might be able to obtain a better understanding of liquid-liquid transitions in general. Naturally, most attempts at trying to answer the latter question have involved the use of water models. In addition to several versions of the ST2 model, a LLCP has also been found in the TIP4P water model[14], TIP4P/2005[15], TIP4P-EW[16], TIP4P/Ice[17], TIP5P[18], and the TIP5P-E model[19]. However, not all water models display this behavior. For example, no LLCP has been found in the SPC/E model[20] nor in the mW model[21,22].

These models are all quite complex and were developed to describe experimental water as accurately as possible. To better understand the physics behind LLCPs, additional studies have been done on much simpler models that simulate monatomic molecules interacting via a simple pair-interaction[23–34]. These studies indicate that for a LLPT to occur, there needs to be a competition between two liquid structures of different density; a collapsed high-density liquid (HDL) and an expanded low-density liquid (LDL). Typically, the LDL state is glassy and more structured, while the HDL state is disordered and far less viscous. These results imply that there might be strong connection between the occurrence of two competing liquid states and the glass transition[4,20,35–37].

LLCPs have been mainly found in models of tetrahedral liquids, and a significant amount of research has been done on the critical behavior in this type of liquid. For instance, a study by Smallenburg et al. using a general model of tetrahedrally coordinated liquids found that making the bond angle more flexible affects the relative stability of the liquid and crystal phases[38]. When the bond angle flexibility is increased, the LLCP moves to a different temperature and ultimately disappears.

Tetrahedral network-forming liquids such as water, liquid silica, liquid silicon, and liquid germanium display a range of anomalies not found in other liquids, and the existence of an LLCP may explain the presence of these anomalies. For example, the density anomaly in water (i.e. the density of liquid water *increases* upon heating) could be explained in terms of the competition between a tetrahedral structure and a distorted structure[3]. Near the density anomaly, the high-density distorted structure becomes more favorable as we increase the temperature, and thus the overall density goes up. At temperatures much higher or much lower than where the anomaly occurs, only one liquid structure dominates and no such anomaly occurs. Having a region in the phase diagram with two competing liquid structures means there is a possibility for a liquid-liquid phase transition (LLPT) and therefore many models with water-like anomalies also display a LLPT.

LLPTs are not merely a theoretical concept. Since the original discovery of a LLCP in ST2 water, liquid-liquid transitions have been experimentally observed in several one-component systems. In 2000, Katayama et al. found a LLPT in liquid phosphorous[39–41] after simulations indicated the possibility of a transition between a polymeric network-forming liquid and a molecular liquid of P_4 molecules[42–44]. Experimental evidence for the existence of a LLPT in triphenyl phosphate was provided by Shimizu et al. in 2014[45–48]. More recently, in 2020, Henry el al. discovered a first-order LLPT in sulfur[49]. It is quite possible that LLPTs exist in many other one-component systems but obtaining experimental evidence is difficult since a LLPT is typically found deep in the supercooled region of the phase diagram where the LDL and HDL

liquids are meta-stable with respect to a stable crystal.

Although one-component liquid-liquid transitions have been studied for decades, the general underlying mechanisms that cause these transitions remains poorly understood, and more studies with a larger variety of models would help. In this manuscript we consider a modified version of the so-called WAC model. The original WAC by Woodcock, Angell, and Cheeseman is a model of silica (SiO_2) and consists of a 1:2 mixture of Si^{+4} and O^{-2} ions that interact via electrostatics and a Buckingham potential[50]. Surprisingly, the original WAC model is remarkably close to having a LLCP without actually having one[51]; slightly reducing the charge to $Si^{+3.36}$ and $O^{-1.68}$ introduces a LLCP that is easily observable[52,53].

It is hard to compare the charge-modified WAC model to water models such as ST2 and TIP4P, since WAC silica is a mixture of individual ions as opposed to a mixture of H_2O or SiO_2 molecules. Hence, a natural question to ask is *how much do intramolecular bonds affect the existence of a LLCP?* We present here a study of how the LLCP in the charge-modified WAC model of Ref. 52 is affected by the addition of water-like bonds, i.e., creating explicit SiO_2 molecules mimicking the structure of H_2O molecules.

We must emphasize here that we are not trying to model any experimental system; we are simply adjusting the parameters of an extensively studied model with the goal of obtaining a better understanding of what affects the existence of a LLCP. For those readers more interested in an accurate model of experimental silica, we must note that the WAC model is one of the oldest molecular dynamics models of silica and that newer models are available. In particular, the BKS model by van Beest et al.[54] is considered the silica model that provides the best results on structural and mechanical properties[55]. Both BKS and WAC reproduce the pair distribution functions well, but BKS has far better experimental agreement of the mechanical moduli of the crystalline polymorphs because it employs fractional charges on its ions as well as a slightly different interaction potential[55,56]. Of course, the charge-modified WAC model also employs fractional charges, but its interaction potential is the same as that of the original WAC model and therefore does not accurately reproduce the properties of experimental silica. It is interesting to note that both BKS and the original WAC model show hints of a possible LLCP at low temperatures[57–59] although more recent studies suggest that there is no LLCP in BKS[51,60].

II. METHODS

The bonded modified WAC model is defined by an interaction potential that consists of three terms,

$$U(r_{ij}) = \frac{1}{4\pi\varepsilon_0}\frac{f_q^2 q_i q_j}{r_{ij}^2} + A_{ij}\exp(-B r_{ij}) + U_{\text{bonds}} \qquad (1)$$

where subscripts $i, j = \{\text{Si}, \text{O}\}$ indicates the ion type. The first term represents the electrostatic interaction between the ions, the second term the ion-ion repulsion due to interpenetration of electron shells[61], and the third term represents the intramolecular bonds. The parameters we use here are the same as in the original WAC model[51,55]: $A_{\text{Si,Si}} = 1.917\,991\,469 \times 10^5$ kJ/mol, $A_{\text{Si,O}} = 1.751\,644\,217 \times 10^5$ kJ/mol, $A_{\text{O,O}} = 1.023\,823\,519 \times 10^5$ kJ/mol, and $B = 34.48\ \text{nm}^{-1}$. The original WAC model does not have explicit bonds (i.e., $U_{\text{bonds}} = 0$) and has ion charges equal to $+4e$ and $-2e$ (i.e., $f_q = 1$). In this study we shall focus on the version with 84% of the original charge (i.e., $f_q = 0.84$) such that the ions have charge $+3.36e$ and $-1.68e$, sometimes referred to as the mWAC model. This version has an easily accessible LLCP as demonstrated in previous studies[52,53].

For the intramolecular interactions we use a harmonic potential, which is also used in many of the water models:

$$U_{\text{bonds}}(r,\theta) = \tfrac{1}{2}k_r(r-r_0)^2 + \tfrac{1}{2}k_\theta(\theta-\theta_0)^2 \qquad (2)$$

The first term in this equation adds an energy penalty whenever an intramolecular Si-O bond r deviates from its natural length r_0, while the second term adds a penalty whenever the intramolecular O-Si-O angle θ deviates from the natural angle θ_0. Large values for the harmonic force constants k_r and k_θ should lead to rigid Si-O bonds and rigid O-Si-O angles, respectively. Conversely, small values produce a more flexible model, and in the limit that $k_r \to 0$ and $k_\theta \to 0$ we should recover the original non-bonded WAC model.

Instead of using Eq. 2 to restrain the bond length and bond angle, we can also fix the Si-O and O-O distance within each SiO_2 molecule using an algorithm such as SETTLE[62], RATTLE[63], or SHAKE[64]. Using these algorithms, the Si-O and O-O distances are kept at a fixed value which basically sets the stiffness parameters to $k_r = k_\theta = \infty$. For all simulations where we keep the bond angle and bond length fixed (i.e. rigid bonds), we use here the SETTLE algorithm.

All Molecular Dynamics simulations are done using Gromacs 4.6.7, which is an old version of Gromacs[65]. In newer versions such as Gromacs 2022, the superior "Verlet cutoff-scheme" is used instead of the older "group cutoff-scheme". Unfortunately, the Verlet cutoff-scheme does not (yet) support the Buckingham potential, which means that we cannot simulate the WAC model using Gromacs version 5.0 or higher[66]. The use of an old version of Gromacs does not affect the quality of our data, but it does reduce the speed of our simulations. Furthermore, installation of such an old version of the software is not straightforward. Gromacs contains highly optimized code, and we found it necessary to turn off the "hardware acceleration" option in order for Gromacs 4.6.7 to compile correctly[67].

It is important to run each simulation long enough to ensure that the system has reached a meta-stable equilibrium. We denote the average time needed to reach equilibration by τ. For the non-bonded WAC model we use the same convention as in Ref 52: $\tau = \sqrt{\langle r_{\text{O}}(t)^2\rangle} = 0.56$ nm, i.e., the average time it requires for an O ion to move twice its diameter of 0.28 nm. For the bonded models it is more appropriate to consider the diffusion D of the whole SiO_2 molecule instead of that of just the O ion. The diameter of a SiO_2 molecule depends on the Si-O bond length r_0 and is approximately equal to the diameter of an O atom plus twice the Si-O bond length: $(0.28\ \text{nm}) + 2r_0$. For the bonded models we therefore use $\tau = \sqrt{\langle r_{\text{SiO}_2}(t)^2\rangle} =$

$(0.56\text{ nm}) + 4r_0$, i.e., the average time it requires for a SiO_2 molecule to move twice its diameter.

To quickly determine if a model has a LLPT, we measure the pressure $P(T,\rho)$ for several temperatures T along isochores of density $\rho = 1.5, 1.6, \ldots, 2.6$ g/cm^3. A liquid-liquid coexistence region exists where one or more isochores cross, since at that state point (T,P) we have multiple densities coexisting in a meta-stable equilibrium. We start each isochore at a high temperature of 12000 K (12 kK) and sequentially run simulations at lower and lower temperatures. Each simulation runs for at least 3τ: an equilibration run of time $t_{\text{eq}} = \tau$ followed by a production run of at least $t_{\text{prod}} \geq 2\tau$.

As the simulations are performed along isochores, we employ the constant-volume/constant-temperature (NVT) ensemble. Each simulation is done with $N = 500$ SiO_2 molecules. The v-rescale thermostat[68] is used to keep the temperature constant, and the PME Ewald sum is used for the electrostatics calculations. We found that a molecular dynamics time step of 1 fs is sufficiently small to produce correct results.

At low pressures, below 0 GPa, the liquid is in a metastable equilibrium with the vapor. When the pressure is lowered further, we ultimately reach the liquid's stability limit (the *liquid-vapor spinodal*), where we find vapor bubbles spontaneously nucleating in the bulk liquid. The formation of these bubbles is readily detected in the simulation: when using the NVT ensemble, the sudden formation of a bubble relieves the tension, causing the pressure of the system to quickly jump up to a less negative value. When we witness such a jump, it is clear we have crossed the spinodal. By tracking at which state points (T,P) these jumps occur, we are able to obtain a rough estimate of the location of the spinodal. The liquid-vapor spinodal is indicated in the isochore plots by a thick gray curve in the negative pressure regime.

At low temperatures, the diffusivity D quickly decreases, making the liquid more glassy. This significantly increases the time τ needed to reach equilibrium, since $\tau \propto D^{-1}$. Most isochores presented here are truncated around $D \approx 10^{-7}$ cm^2/s, which corresponds to a τ of about 30 ns.

III. TYPICAL PARAMETER VALUES

To determine how intramolecular bonds affect the LLCP in the modified WAC model, we vary the parameters k_r, r_0, k_θ, and θ_0 as defined in Eq. 2. However, we must first determine what parameter values should be considered "typical". For instance, a small value for k_r should produce such weak bonds that there is little difference between the bonded model and the non-bonded version, while a larger value for k_r should clearly constrain the intramolecular Si-O distance to a value near r_0.

A. Si-O bond length r_0

To determine the typical value of the natural Si-O bond length r_0, we consider in Fig. 1 the first peak of the radial distribution function $g_{\text{SiO}}(r)$ of the non-bonded charge-modified

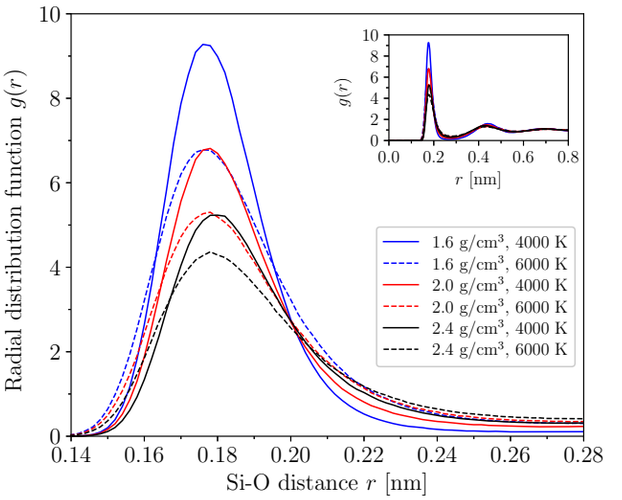

FIG. 1. **Natural bond length r_0 of non-bonded mWAC is 0.18 nm.** First peak of the radial distribution function $g_{\text{SiO}}(r)$ of the non-bonded mWAC model[52] for several temperatures and densities. The maximum of this peak lies around $r \approx 0.18$ nm for all temperatures and densities considered, which means that the typical distance between each Si ion and its nearest O ion is about 0.18 nm. Inset: radial distribution function $g_{\text{SiO}}(r)$ for a larger range of r.

WAC model of Ref. 52. For a wide range of densities and temperatures we find that the distance between an Si ion and its nearest O ion is about 0.18 nm, and we thus conclude that $r_0 = 0.18$ nm is a good reference value for the natural Si-O bond length.

Furthermore, we see in Fig. 1 that the Si-O bond varies between, roughly, 0.16 and 0.21 nm. Based on these observations, we shall use $r_0 = 0.18$ nm when we keep r_0 fixed, and explore the range $r_0 = 0.16, 0.17, \ldots, 0.21$ nm when we vary r_0 to study how the LLCP is affected by r_0.

B. Bond stiffness k_r

To determine a typical value for the bond stiffness k_r, it helps to look at other models for guidance. For instance, the SPC/E water model and the TIP4P water model are two popular water models that use $k_r = 345{,}000$ and $k_r = 502{,}416$ kJ mol^{-1} nm^{-2}, respectively. The OPLS/AA force field, which defines model parameters for a wide variety of molecules, uses k_r values between 177,401 (CT-P bond) and 962,320 (CZ-CZ bond) with most values between 300,000 to 500,000[69]. We should consider a relative strong bond to clearly see how intra-molecular bonds affect the LLCP, and we shall therefore use $k_r = 5\times10^5$ kJ mol^{-1} nm^{-2} as the typical value for k_r.

Increasing the bond stiffness increases the bond vibrational frequency, which might require a smaller time step in our molecular dynamics simulation. To prevent our simulations from being too time-consuming, we will not work with k_r values larger than 2×10^6 kJ mol^{-1} nm^{-2}, which, considering the

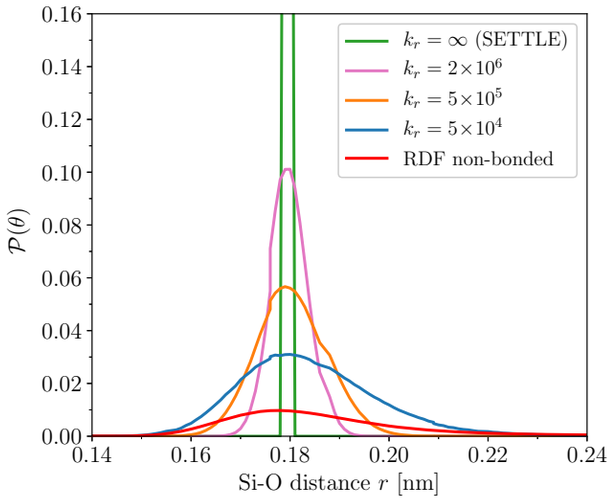

FIG. 2. **Increasing bond stiffness k_r reduces flexibility of Si-O bond length r.** We study several values of k_r, which allows for a range of bond length flexibility. Our lowest value $k_r \approx 5\times10^4$ kJ mol^{-1} nm^{-2} allows the Si-O bond length to fluctuate between 0.15 and 0.22 nm, while the bond length fluctuates far less upon increasing k_r. By applying the SETTLE algorithm[62] we can fix the bond length to 0.18 nm, effectively setting $k_r = \infty$. All curves shown are at 2.0 g/cm^3 and 4000 K. For comparison, we include the first peak of the radial distribution function $g_{\mathrm{SiO}}(r)$ of the non-bonded mWAC model (in red).

OPLS/AA parameters, can be considered an extremely stiff bond.

Decreasing the bond stiffness too much will also lead to problems. In particular, we find that using a k_r value less than 5×10^4 causes the Gromacs 4.6.7 program to crash, which most likely happens when two bonded atoms move too far away from each other, causing problems for the domain decomposition algorithm.

In Fig. 2 we demonstrate how k_r affects the bond length r_0. For these simulations we turn off the angular constraint by setting $k_\theta = 0$, which also means that the value of θ_0 is ignored and thus irrelevant. As expected, increasing the bond stiffness k_r reduces the variance in bond length. We find that a value of about $k_r \approx 5\times10^5$ kJ mol^{-1} nm^{-2} is sufficient to restrain the bond length to $r = 0.18 \pm 0.01$ nm (full width at half maximum).

C. O-Si-O bond angle θ_0

Since SiO_2 is a tetrahedral liquid, and the structure of the liquid in the modified WAC models has indeed a tetrahedral structure[52], we shall consider here the tetrahedral angle 109.47° as the typical value for θ_0. As mentioned earlier in the introduction, the tetrahedrality in some liquids seem to allow for the existence of two separate liquids; a low-density liquid with a tetrahedral structure and a high-density disordered structure. When these are able to phase-separate, a LLPT may occur. However, it is an open question if this phenomenon also occurs with liquids that do not possess a tetrahedral structure. For this reason we consider the angles $\theta_0 = 90°$, 100°, 109.47°, and 120° to see how the intramolecular angle affects the LLCP.

D. Bond angle stiffness k_θ

To establish the relevant range of values for the angle stiffness k_θ we shall consider again the parameters used in other models. Most k_θ values in the OPLS/AA force field are between 250 and 800 kJ mol^{-1} rad^{-2}, with the largest value around 1445. The SPC/E water model has $k_\theta = 383$ kJ mol^{-1} rad^{-2} while TIP4P uses $k_\theta = 628$ kJ mol^{-1} rad^{-2}. Based on these numbers, we employ $k_\theta = 500$ kJ mol^{-1} rad^{-2} as our typical value.

With Fig. 3 we confirm that our values for k_θ produce the correct behavior. When $k_\theta = 0$ there is no angular restraint and we find a wide distribution of angles, as shown in Fig. 3a. In Figs. 3b and 3c we use the tetrahedral angle of $\theta_0 = 109.47°$ and find the range of angles to be much more restrained. With $k_\theta = 500$ the variance is about $\theta_0 \pm 30°$ while $k_\theta = 2000$ kJ mol^{-1} rad^{-2} restrains the angle to approximately $\theta_0 \pm 20°$. When we use the SETTLE algorithm[62] instead of the harmonic bonds of Eq. 2 we fix the bond angle to θ_0 and the variance is minimal. This is equivalent to setting $k_\theta = \infty$.

IV. RESULTS AND DISCUSSION

A. Non-bonded vs bonded mWAC

Now that we have established the best parameter values to use, we are ready to study how varying these parameters affect the LLCP in mWAC. In Fig. 4 we compare the isochores of the non-bonded mWAC model to the isochores of the bonded model with increasing values of bond stiffness.

We first compare the non-bonded mWAC model in Fig. 4a with the most-flexible version of the bonded model in 4b, which has no restraint on the angle ($k_\theta = 0$) and the smallest possible value for the bond stiffness ($k_r = 5\times10^4$ kJ mol^{-1} nm^{-2}). One would expect that such very weak bonds have little to no effect at all on the phase diagram, and we find that this is more or less the case. The LLCP does shift a little to lower temperatures, and at high temperatures the isochores shift to lower pressures as well.

As we increase the bond and angle stiffness to $k_\theta = 500$, $k_r = 5\times10^5$ we see in Fig. 4c that the LLCP moves to further to a lower temperature, a higher pressure, and a lower diffusivity, making it more difficult to access the LLCP with our simulations. This behavior continues as we increase the stiffness to $k_\theta = 2000$ and $k_r = 2\times10^6$ (not shown), until we can barely see the isochores cross when we have rigid bonds and keep the Si-O bond length and O-Si-O angle fixed at $r_0 = 0.18$ nm and $\theta_0 = 109.47°$ ($k_\theta = k_r = \infty$).

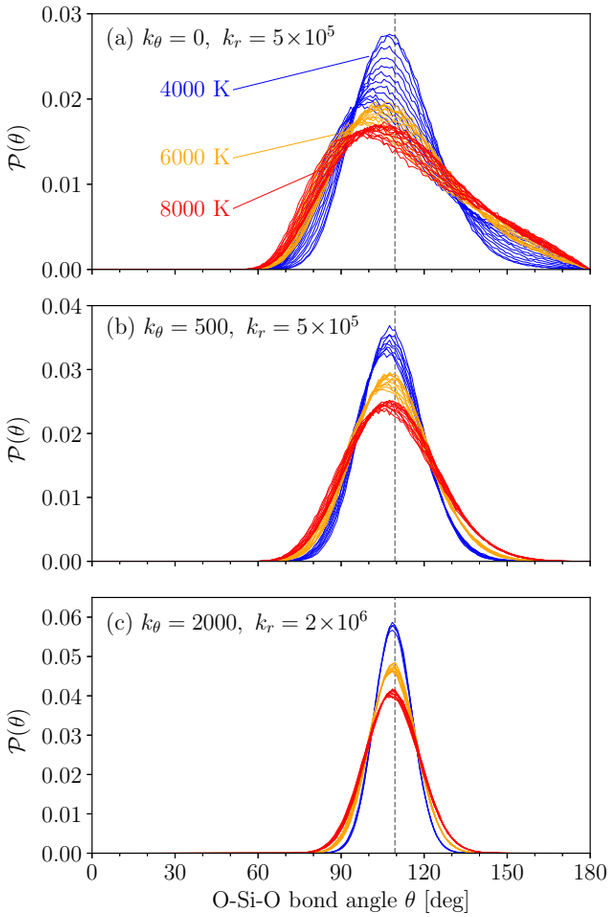

FIG. 3. **Increasing angle stiffness k_θ reduces flexibility of O-Si-O bond angle θ.** The probability distribution of θ for several temperatures (blue: 4000 K, orange: 6000 K, red: 8000 K) and several densities ($\rho = 1.5, 1.6, \ldots, 2.6$ g/cm^3; lowest density has the highest peak). In all cases the natural bond angle is $\theta_0 = 109.47°$, indicated by the vertical dashed line. Bond length is kept at $r_0 = 0.18$ nm with k_r as indicated. (a) When $k_\theta = 0$ there is no angular restraint, which leads to a wide distribution of angles around θ_0. (b) With $k_\theta = 500$ kJ mol^{-1} rad^{-2} the angles are restrained to $\theta_0 \pm 30°$, approximately. (c) Using $k_\theta = 2000$ kJ mol^{-1} rad^{-2} we restrain the angles to $\theta_0 \pm 20°$.

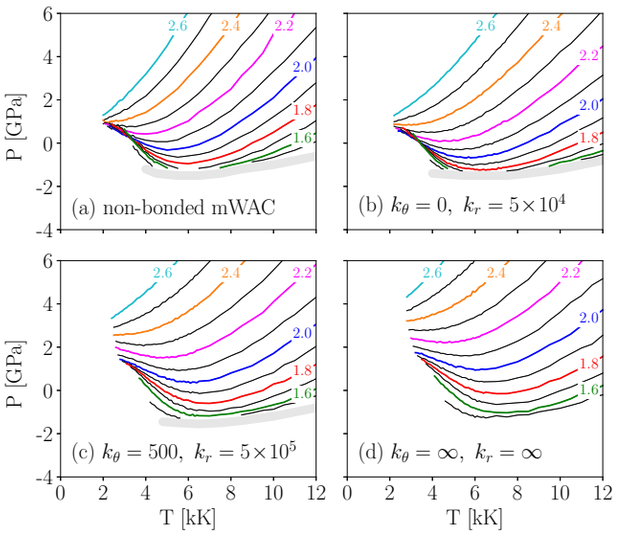

FIG. 4. **Adding bonds and increasing bond stiffness slightly reduces the accessibility of the LLCP.** (a) The original modified-WAC model with $f_q = 0.84$ displays a clear LLCP near $(T,P) = (3350\text{ K}, 0.19\text{ GPa})$[53]. (b) Introducing weak bonds moves the LLCP to a slightly lower temperature, but leads to no other significant changes in the phase diagram. (c) Increasing the stiffness k_r of the Si-O bond and/or the stiffness k_θ of the O-Si-O angle, causes the LLCP to move to lower T and higher P. (d) With rigid bonds ($k_r = k_\theta = \infty$) the LLCP moves to such low temperatures that we can barely detect the crossing of isochores.

B. How bond length r_0 affects the LLCP

Fig. 5 shows what happens when we adjust the bond length r_0 while keeping the bond stiffness fixed to $k_\theta = 500$ and $k_r = 5\times10^5$. Our reference value for r_0 is 0.18 nm, which is shown in Fig. 5c and is identical to Fig. 4c. When we reduce the bond length from 0.18 nm to 0.17 nm (Fig. 5b) the LLCP moves to a higher pressure and lower temperature. This is similar to what happens when we increase the bond stiffness, but evidently the effect is much stronger when we change r_0. When $r_0 =$ 0.17 nm the LLCP also moves to a smaller diffusivity (below $D = 10^{-7}$ cm^2/s), which means that the simulations require such a long time to reach 3τ that we are no longer able to confirm that there is indeed a LLCP. Reducing the bond length even further, we find that for $r_0 = 0.16$ nm (Fig. 5a) it is no longer clear that the isochores will cross, and thus this version of the model is likely not to have a LLCP at all.

Increasing the bond length has the opposite effect. As we increase r_0 from 0.18 nm (Fig. 5c) to 0.19 nm (Fig. 5d), and then to 0.20 nm (Fig. 5e) we find that the LLCP becomes more and more accessible; it moves to a higher temperature, a lower pressure, and a higher diffusivity. For $r_0 = 0.20$ nm the critical point is around $(T,P) = (4300\text{ K}, -0.9\text{ GPa})$, where we have the 1.6 g/cm^3 isochore cross with the 2.0 g/cm^3 isochore. At that point, the low-density isochore has a diffusivity of $D \approx 4.0\times10^{-6}$ cm^2/s, while the high-density isochore is about 1.3×10^{-5} cm^2/s, which is more than 3 times larger. This observation agrees with the general observation that the low-density liquid (LDL) state is always less "fluidic" (less diffusive and more structured) than the high-density liquid (HDL) state of a LLPT[4,20,32,33,35–37].

Upon further increase of the bond length, the LLCP continues to move to higher temperatures and lower pressures, and eventually moves below the liquid-vapor spinodal (thick gray curves in Fig. 5), thus becoming inaccessible again. In Fig. 5f we see that when $r_0 = 0.21$ nm the LLCP is still visible, but barely above the spinodal.

That r_0 strongly affects the diffusivity D near the LLCP is an important observation. First of all, when a liquid has a larger diffusivity, less time is needed to equilibrate it, which

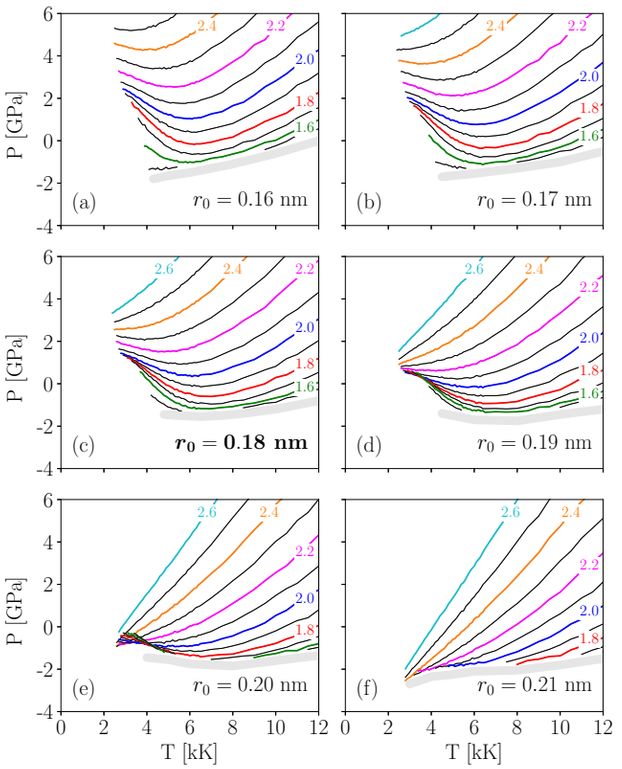

FIG. 5. **Bond length r_0 strongly affects the LLCP.** Isochores of the bonded mWAC model with changing r_0, while keeping the remaining bond parameters constant at $k_\theta = 500$, $k_r = 5\times10^5$, and $\theta_0 = 109.47°$. (a) When the Si-O bond is very short (0.16 nm) a LLCP is no longer visible. (b) At 0.17 nm, the isochores converge near $T \approx 3000$ K, $P \approx 1.8$ GPa, $\rho \approx 1.8$ g/cm^3, even though a clear crossing is not yet visible. (c) At our reference value of $r_0 = 0.18$ nm, the LLCP can be found at the edge of our simulations, at a diffusivity close to 10^{-7} cm^2/s. The location of the LLCP is roughly at (3000 K, 1.3 GPa, 1.8 g/cm^3). (d) Increasing the bond length to 0.19 nm makes the LLCP more accessible, near (3500 K, 0.4 GPa, 1.8 g/cm^3). (e) At 0.20 nm the LLCP has moved to a higher temperature and a lower pressure: (4300 K, -0.9 GPa, 1.8 g/cm^3). (f) Increasing r_0 to 0.21 nm moves the critical point below the liquid-vapor spinodal (thick gray line). The highest temperature at which we find isochores cross is near (4700 K, -1.8 GPa, 2.0 g/cm^3).

means that the LLCP is easier to study using simulations. Secondly, the diffusivity plays an important role in crystallization. A liquid with a large diffusivity might crystallize faster, as the growth rate $R(T)$ of the crystal is typically proportional to the diffusion constant $D(T)$. At temperatures well below the melting point, the growth rate can be described by the Wilson-Frenkel model:

$$R(T) = c\,D(T)\,[1 - \exp(-\Delta G(T)/k_bT)] \qquad (3)$$

Here $\Delta G(T)$ is the difference in free energy between the liquid and crystalline phases, and c a constant[70–73].

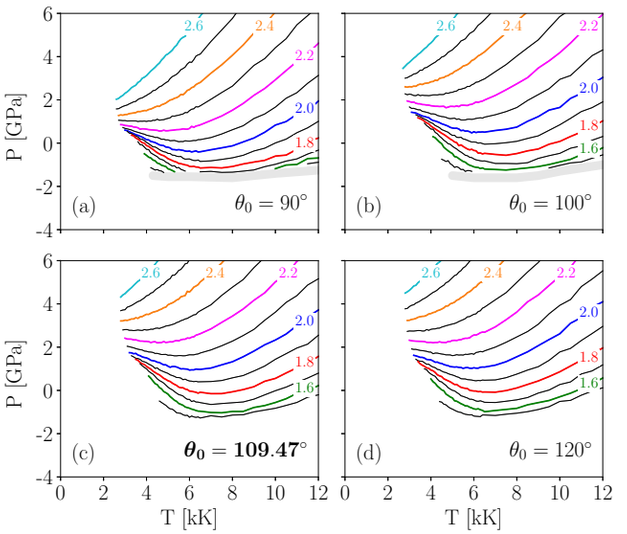

FIG. 6. **Natural bond angle θ_0 has minimal effect on the LLCP.** Isochores for several values of θ_0 with rigid bonds ($k_\theta = k_r = \infty$). Upon increasing θ_0 the LLCP moves only slightly to lower temperatures and higher pressures. (a) Isochores for $\theta_0 = 90°$. (b) Isochores for $\theta_0 = 100°$. (c) Isochores for $\theta_0 = 109.47°$. (d) Isochores for $\theta_0 = 120°$.

C. How bond angle θ_0 affects the LLCP

The non-bonded mWAC model naturally forms a tetrahedral structure at low temperatures. This is clear, for instance, from the distribution of O-Si-O angles in Fig. 3a, which shows a broad peak around the tetrahedral angle of 109.47° at low temperatures and low densities. In Fig. 6 we consider what happens when we change the bond angle from 109.47° to 90°, 100°, or 120°. Since rigid bonds ($k_\theta = \infty$) has the largest effect on the LLCP (see Fig. 4), we will use $k_\theta = \infty$ to enhance the effect of changing θ_0. The results for $k_\theta = 500$ and $k_\theta = 2000$ are similar, but less pronounced.

As we move from 90° (Fig. 6a), to 100° (Fig. 6b), then 109.47° (Fig. 6c), and finally 120° (Fig. 6d), we find that the LLCP moves only slightly to lower temperatures and higher pressures. The effect is minimal, especially in comparison to the impact that r_0 and f_q have on the LLCP.

In Fig. 6 we do see that increasing θ_0 moves the isochores to a higher pressure. This means that at a given state point (T, P), increasing θ_0 causes the density to decrease and thus the liquid to expand. Hence, a more open O-Si-O angle expectedly gives rise to a more open, expanded structure. However, Fig. 6 suggests that this expansion happens equally for LDL (low density) as for HDL (high density), so there is no net movement of the LLCP.

D. Si/O coordination numbers

That the O-Si-O bond angle has such little effect on the LLCP is surprising, as the (tetrahedral) structure of the liquid is ex-

pected to play a significant role regarding the presence of a LLCP. To better understand what is happening to the liquid structure as we change r_0 or θ_0, we consider in Figs. 7 and 8 the Si and O coordination numbers. The coordination number n_O is the average number of O ions within the first coordination shell surrounding a Si ion:

$$n_O \equiv 4\pi\rho_O \int_0^{r_{min}} r^2 g_{SiO}(r)\,dr \tag{4}$$

Here ρ_O is the number density of the O ions, $g_{SiO}(r)$ the Si-O radial distribution function, and r_{min} the location of its first minimum. The coordination number n_{Si} is the average number of Si ions surrounding each Si, and has the same definition as n_O but with ρ_{Si} and $g_{SiSi}(r)$.

We see in both Fig. 7 and Fig. 8 that for low temperatures and low densities the coordination numbers approach $(n_O, n_{Si}) = (4,4)$ which indicates a tetrahedral structure where each Si has four nearest O neighbors that each connect to one other Si, thus resulting in four Si ions around each Si. As we increase the temperature and/or density, the probability of finding a fifth O ion inside the Si first coordination shell increases, and with that the probability of finding additional Si neighbors, beyond the tetrahedral four.

The average number of Si ions and O ions around each Si ion varies for each state point (ρ, T), however, there appears to be a strict lower bound on the ratio n_{Si}/n_O as indicated by a black dashed line in each panel of Figs. 7 and 8. Note that the slope of this lower bound line depends strongly on the value r_0 but is practically the same for all values of θ_0, thus hinting to a correlation between the location of the LLCP and this slope. When the slope of the lower bound line is above $\sim$3.4 (as for $r_0 = 0.16$) the corresponding isochores no longer cross, and the LLCP disappears. If the slope is below $\sim$2.7 (as for $r_0 = 0.21$) the LLCP disappears below the liquid-vapor spinodal line. Hence, the LLCP only exists when the slope of the lower bound line is approximately within the range of [2.7, 3.4]. The range of slope values was also found by Ref.[52] upon changing the ion charge by varying f_q. It is unclear if this range is specific to only this family of models, or if these are universal values which are true for other models as well.

Plots of n_{Si} vs. n_O provide a useful tool for studying the liquid structure. However, it can be difficult to accurately estimate the slope of the lower bound line. Furthermore, we are mostly interested in the number of *additional* Si ions per *additional* O ion, not the total number of Si and O ions. Let us therefore define $R_{Si/O}$ as the number of additional Si ions (beyond the tetrahedral four Si) per additional O ion (beyond the tetrahedral four O):

$$R_{Si/O} \equiv \frac{n_{Si} - 4}{n_O - 4} \tag{5}$$

This ratio is well-defined for any pair of coordination numbers (n_O, n_{Si}), except when there are exactly zero additional O ions. When $n_O \approx 4$ it is possible for $R_{Si/O}$ to become unrealistically large, and we therefore omit the few state points in Figs. 7, 8, and 9 that have $n_O \leq 4.1$.

In Fig. 9 we present the same data as in Fig. 7, but now with the value of $R_{Si/O}$ as a function of temperature T. The

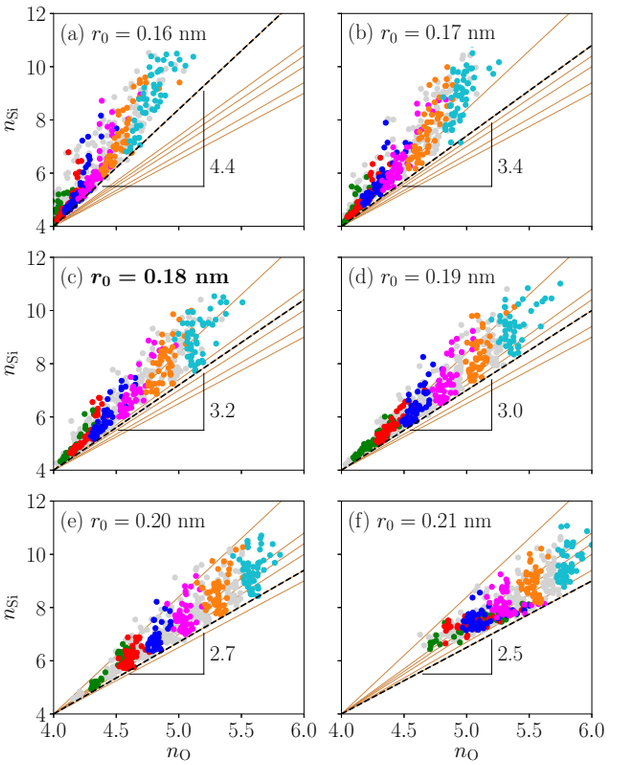

FIG. 7. **Varying r_0 strongly affects Si/O coordination numbers.** Si coordination number n_{Si} vs. O coordination number n_O, for varying r_0 and fixed $\theta_0 = 109.47°$, $k_\theta = 500$, $k_r = 5\times10^5$. Panel (a) corresponds to the same bond parameters as those in Fig. 5a, and similarly for all other panels (b)-(f). Different colors indicate different densities, matching those in Fig. 5. (a) When $r_0 = 0.16$ nm we have a large increase in n_{Si} upon increasing n_O, thus giving a lower bound line of slope $\sim$4.4. At this value for r_0 there is no LLCP. (b) Increasing r_0 to 0.17 nm reduces the slope to $\sim$3.4, which corresponds to the isochores converging in Fig. 5b. (c) When $r_0 = 0.18$ nm the lower bound line has a slope of $\sim$3.2 and a clear LLCP is visible in Fig. 5c. (d) Coordination numbers for $r_0 = 0.19$ nm, with a clear LLCP in Fig. 5d. (e) Coordination numbers for $r_0 = 0.20$ nm, with a clear LLCP in Fig. 5e. (f) At $r_0 = 0.21$ nm the lower bound line has a slope less than $\sim$2.7 and the LLCP disappears below the liquid-vapor spinodal in Fig. 5f.

minimum value of $R_{Si/O}$ in these plots is identical to the slope of the lower bound lines in Fig. 7. These figures show that the behavior of $R_{Si/O}$ correlates very strongly with the location/existence of the LLCP. Interestingly, even at state points far away from the LLCP (at high temperatures) the fluctuations of $R_{Si/O}$ correlate to what happens at lower temperatures. In particular, for $r_0 = 0.16$, which does not have a LLCP, the value of $R_{Si/O}$ fluctuates around large values, between 5 and 10. For the models that display a clear LLCP, such as $r_0 = 0.19$ and 0.20, the value of $R_{Si/O}$ fluctuates around much smaller values, between 3 and 6. When the LLCP starts to disappear below the liquid-vapor spinodal, the value of $R_{Si/O}$ fluctuates even less: in Fig. 9f all values lie between 2.5 and 4.5.

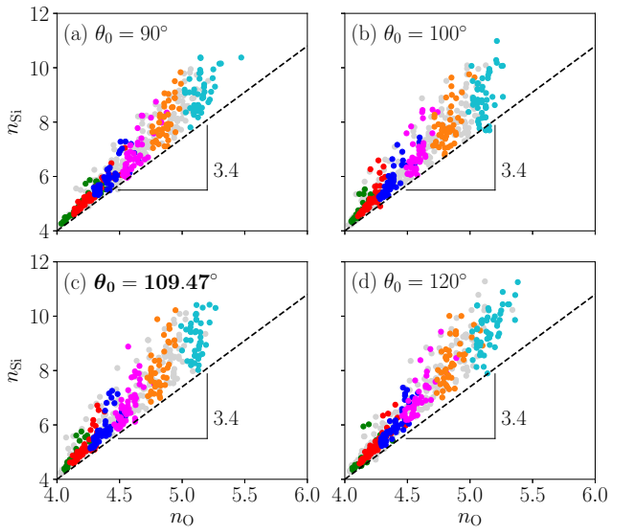

FIG. 8. **Varying θ_0 barely affects Si/O coordination numbers.** Si coordination number n_{Si} vs. O coordination number n_O, for varying θ_0 and fixed $r_0 = 0.18$ nm with rigid bonds ($k_\theta = k_r = \infty$. Panel (a) corresponds to the same bond parameters as those in Fig. 6a, and similarly for all other panels (b)-(f). Different colors indicate different densities, matching those in Fig. 6.

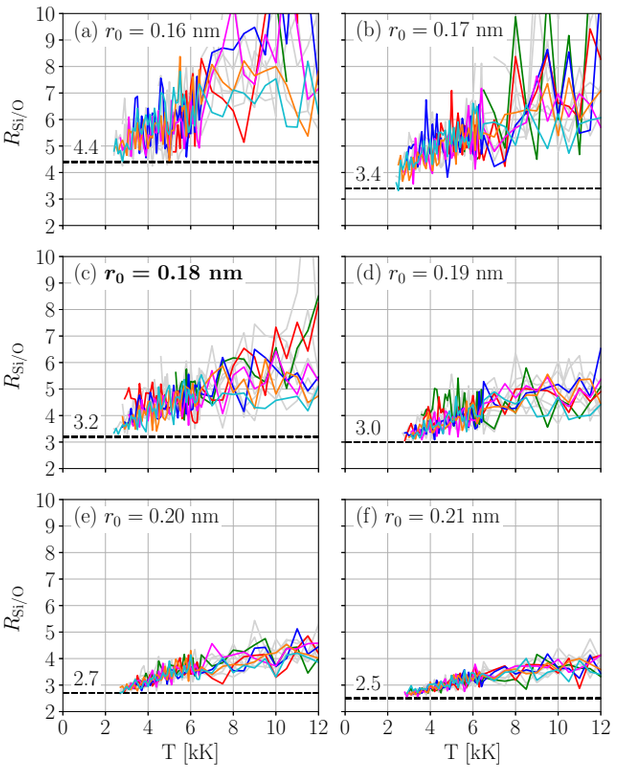

FIG. 9. **Plots of $R_{Si/O}$ vs. temperature T as alternative to n_{Si} vs. n_O plots.** Number of additional Si ions per additional O ion $R_{Si/O} = (n_{Si} - 4)/(n_O - 4)$, as a function of temperature T. For clarity, state points with $n_O \leq 4.1$ have been omitted. Panel (a) corresponds to the same bond parameters as those in Figs. 5a and 7a, and similarly for all other panels (b)-(f). Different colors indicate different densities, matching those in Fig. 5 and 7. Black dashed lines indicate lower bounds of $R_{Si/O}$ and are identical to the black dashed lines in Fig. 7. Plotting $R_{Si/O}$ vs. T makes it easier to determine the lower bound of $R_{Si/O}$ (i.e. the slope of the lower bound line in Fig. 7), and shows more clearly the behavior of the coordination numbers as the temperature decreases.

E. Gibbs free energy of mixing

Why $R_{Si/O}$ correlates so strongly with the presence of a LLCP can be explained by considering the Gibbs free energy of mixing, $\Delta G_{mix} = \Delta H_{mix} - T\Delta S_{mix}$. As has been done for water[74–77], we can consider the liquid as a mixture of LDL and HDL, with their ratio controlled by a thermodynamic equilibrium. When $\Delta G_{mix} < 0$ the liquid will remain homogeneous for all temperatures and pressures, but when $\Delta G_{mix} > 0$ the mixed state is not the preferred state, and the liquid will spontaneously phase separate, allowing for a LLPT to appear.

Consider the model with $r_0 = 0.20$, where the O ions are relatively far from their bonded Si ion. Because of this large distance, when a fifth O enters the first coordination shell of a Si, it will not bring as many Si ions with it into the shell, since the long bonds keep these additional Si ions outside the shell. The result is a fairly low number of additional Si ions per additional O ion, in other words a relatively small value for $R_{Si/O}$ as in Fig. 9e. Because the number of ions in the coordination shell does not increase significantly when an extra O ion moves into the shell, the change in entropy is not large either. Thus, S_{mix} remains small enough for $\Delta G_{mix} > 0$ for certain values of T, which allows for the liquid-liquid phase separation to occur (see Fig. 5e).

On the other hand, when $r_0 = 0.16$, the O ions are close to their bonded Si ion, and when a fifth O ion appears in the first coordination shell of a Si, it drags with it a large number of additional Si ions. The result is a much larger value for $R_{Si/O} = (n_{Si} - 4)/(n_O - 4)$ as is visible in Fig. 9a, and thus a relatively large change in entropy. In this situation the S_{mix} becomes large enough such that $\Delta G_{mix} < 0$ for all T, and the LLCP does not appear (see Fig. 5a).

F. Comparison to other models of tetrahedral liquids

As mentioned in the introduction, a significant amount of research has been done on the critical behavior in tetrahedral liquids using other models than WAC. Many of these tetrahedral models consist of particles that have an explicit tetrahedral interaction between them. For instance, in the tetramer model by Smallenburg et al.[38] each particle consists of five hard spheres: one central sphere surrounded by four spheres that act like 'arms' oriented along a tetrahedral geometry. Each arm has an attractive patch on its surface which allows it to bond with the arms of other particles. It is possible to adjust the flexibility of the tetramer bonds by adjusting the size of these patches and how much the arms are allowed to deviate

from the ideal tetrahedral angle of 109.47°. Ref. 38 finds that increasing the rigidity (i.e., decreasing the flexibility) introduces a region with a stable liquid-liquid coexistence. However, further increase of the rigidity changes this LL coexistence to a meta-stable state, with the crystal being the stable phase. The arm length in this model can also be adjusted, which is similar to changing r_0 in our modified WAC model. Ref. 38 finds that, generally, an increase in arm length causes the critical temperature T_c to increase. Fig. 5 of this paper displays a similar behavior in the modified WAC model when increasing r_0.

Another tetrahedral model of relevance is the modified Stillinger-Weber (SW) model by Molinero et al.[78]. In this model, the particles interact via an interaction potential of the form $v = v_2(r) + \lambda v_3(r,\theta)$ where $v_2(r)$ represents a basic pairwise potential and $v_3(r,\theta)$ is a three-body term which favors tetrahedral coordination by inducing a repulsion for angles that are not tetrahedral. When the repulsion parameter λ is set to $\lambda = 21$ we reproduce the original SW model[79] for liquid silicon, Si, which is known to have a LLCP at negative pressures[80]. Increasing λ decreases the flexibility of the tetrahedral bonds, which promotes the onset of crystallization. On the other hand, decreasing λ increases the flexibility of the tetrahedral bond angle and destroys the LLPT. For instance, Ref. 78 finds that the LL transition no longer occurs at pressure $P = 0$ when $\lambda < 20.25$.

Finally, the tetrahedral model most similar to our modified WAC model is the modified ST2 model by Smallenburg and Sciortino[81]. The original ST2 water model[2] consists of rigid intra-molecular bonds between the oxygen atom O in the center and the two hydrogen atoms H1, H2 and two lone pairs L1, L2 surrounding it. In the modified ST2 model these bonds are allowed to deviate (without an energy cost) by a maximum angle $\theta_{\max}$. Obviously, a larger $\theta_{\max}$ gives rise to more flexible O-H and O-L angles. It is shown in Ref. 81 that more flexible *intra*-molecular angles ∠OH, ∠OL also lead to more flexible *inter*-molecular ∠OOO angles. Furthermore, an increase in flexibility moves the LLCP to slightly lower temperatures, while simultaneously strongly decreasing the melting temperature. Because the melting temperature is much stronger affected than the critical temperature T_c, one finds that at sufficiently large $\theta_{\max}$ the LLCP ultimately moves beyond the melting line and into the stable regime[81].

All three tetrahedral models mentioned above show that the LLCP moves to a lower temperature when the inter-molecular bond angle is made more flexible. It is easy to argue why this makes sense. Near the LLPT there is a competition between two liquid states, the low-density LDL and the high-density HDL. For phase separation to occur, the more structured LDL state needs to possess enough rigidity to distinguish itself from the more fluidic HDL state. Too much fluctuation in the bond angle, and the LDL state becomes (energetically) indistinguishable from the HDL state, leaving us with a single fluid. This is what arguably happens when we increase the temperature of the liquid above the critical temperature T_c — the amplitude of the bond angle fluctuations increases and the separation between LDL and HDL disappears. Hence, if we increase the flexibility of the inter-molecular bond angle via a model parameter, one would naturally expect the T_c to be reached at lower temperatures.

However, we observe in Fig. 4 that the LLCP of the modified WAC moves in the opposite direction; making the Si-O bond angle more flexible (by decreasing k_r and k_θ) causes the LLCP to move to *higher* temperatures instead.

To better understand the similarities and differences between modified WAC and the other tetrahedral models, we need to consider the distribution of the tetrahedral inter-molecular Si-Si-Si angle since the flexibility of (the equivalent of) this angle is what we control in the other models.

In Fig. 10 we consider the inter-molecular Si-Si-Si angle. To calculate this angle we use the four nearest Si neighbors of each Si. The resulting histogram generally has two large peaks for this model, one peak near 60° and one broad peak around 109°. The 60° peak arises from HDL liquid structure, while the 109° peak comes from the tetrahedral structure of the LDL. Since we are only interested in the flexibility of the tetrahedral angle, we present in Fig. 10 those state points that mainly consist of LDL, i.e., low density (1.6 g/cm^3) and low temperatures.

It is clear from Fig. 10a that the Si-Si-Si distribution is not affected at all when we adjust the flexibility of the Si-O angle. Note that this is completely different from what was observed in the flexible ST2 model by Ref. 81. In Fig. 10b we find that changing the bond length r_0 has no effect on the tetrahedral angle either. These surprising observations explain the strange behavior of the bonded modified WAC model. Evidently, the bonds in the model do not affect the inter-molecular tetrahedral angle at all, and therefore the behavior found in other models is not what we find in the bonded m-WAC model. Instead, in this model the LLCP seems to be controlled predominantly by the distribution of the electric charge. The bonds do affect the distribution of charge when r_0 is changed — as indicated by the Si/O coordination numbers discussed in Sec. IV D — but they do not seem to affect the LLCP *directly* as is the case with the other tetrahedral models.

We conclude that the bonded modified-WAC model clearly behaves very differently than any other model studied so far, thus highlighting its importance for the general study of LLCPs. It would be interesting to see in future research how one could adjust WAC to make it more like the other models, which is perhaps possible by changing the van der Waals interaction from Buckingham to e.g. Lennard-Jones.

V. CONCLUSIONS

We have successfully extended the modified-WAC model to include intra-molecular bonds. The addition of these bonds did not have a strong effect on the LLCP and its location. Using bonds with a minimal amount of stiffness produces a very similar set of isochores but with the LLCP slightly moved to a lower temperature. Increasing the stiffness of either the bond angle or the bond length moves the LLCP to lower temperatures, but even with rigid bonds ($k_\theta = k_r = \infty$) the LLCP remains accessible and moves only a minor amount compared to the original non-bonded mWAC model. This movement

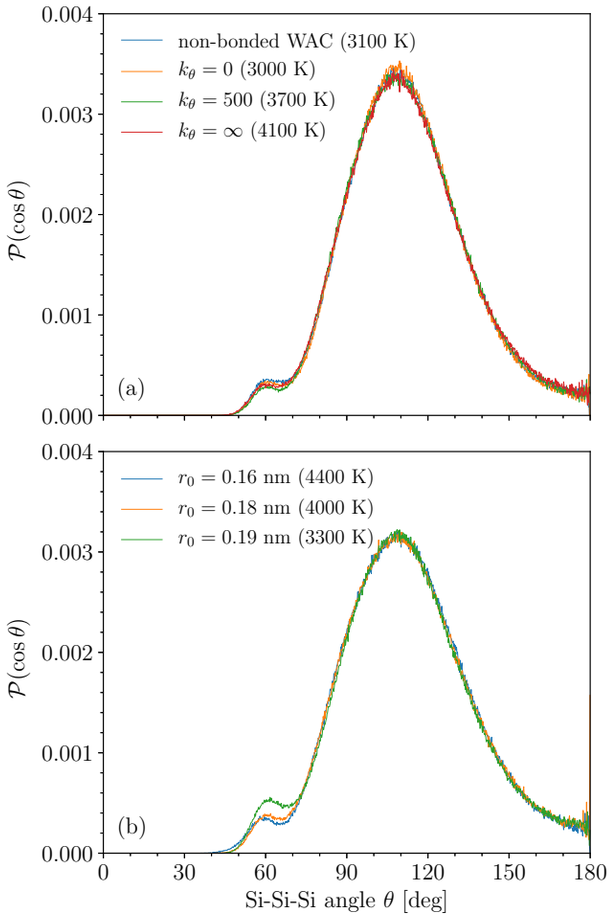

FIG. 10. **Bond angle flexibility k_θ and bond length r_0 do not affect the tetrahedral Si-Si-Si angle.** Probability distribution of $\mathcal{P}(\cos\theta) = \mathcal{P}(\theta)\sin\theta$, with θ the Si-Si-Si angle between the four nearest neighbors of each Si atom. To allow for a valid comparison between different values of k_θ and r_0, we consider here different state points (all at 1.6 g/cm^3) that all produce the same liquid state consisting of mainly LDL. (a) Making the intra-molecular Si-O bond angle less flexible (by increasing k_θ) does not affect the Si-Si-Si bond angle at all, unlike what is observed in other models such as the flexible ST2 model by Ref. 81. (b) Changing bond length r_0 has no effect on the Si-Si-Si bond angle either, even though it significantly affects the LLCP (see Fig. 5). Considering that r_0 does affect the Si/O coordination numbers, we conclude that the electrostatic interaction plays a far more dominant role in this model than the bonds and bond angles do.

is opposite to what happens in other tetrahedral models and can be explained by the observation that adjusting the intra-molecular Si-O bond angle (using k_θ) does not affect the inter-molecular Si-Si-Si angle.

A more significant change occurs when we alter the natural bond length, r_0. Upon decreasing r_0 to around 0.16–0.17 nm the LLCP disappears completely, in a similar fashion as what happens with the original non-bonded WAC model when we increase the charge of each ion by a factor of $f_q = 1.08$[52]. When we *increase* the natural bond length r_0, the LLCP moves to higher temperatures and lower pressures, until at $r_0 = 0.21$ the LLCP disappears below the liquid-vapor spinodal, similar to what happens when we decrease the ion charge by $f_q = 0.72$.

Since increasing r_0 and decreasing f_q have such similar effects, we suspect that both are caused by the same underlying mechanism. Inspection of the Si/O coordination numbers $(n_{\mathrm{Si}}, n_{\mathrm{O}})$ indicates that there is a strong correlation between the location of the LLCP and the number of additional Si ions $R_{\mathrm{Si/O}}$ that enter the first coordination shell of a Si ion when one additional O ion enters the shell. Here $R_{\mathrm{Si/O}} = (n_{\mathrm{Si}} - 4)/(n_{\mathrm{O}} - 4)$, as defined in Eq. 5. When $R_{\mathrm{Si/O}}$ fluctuates between approximately 3 and 5.5 then the model has an accessible LLCP, as is the case for $r_0 \approx 0.19$ nm and $f_q \approx 0.84$. When $R_{\mathrm{Si/O}}$ shows larger fluctuations, e.g. between 5 and 10, then there is no LLPT or LLCP. On the other hand, when $R_{\mathrm{Si/O}}$ shows very small fluctuations between 2.5 and 4 a LLPT might still be visible, but the LLCP moves below the liquid-vapor spinodal line and is no longer accessible. It is quite possible that these ranges for $R_{\mathrm{Si/O}}$ are not universal values, but that they depends on the type of model.

Varying the bond angle θ_0 from 109.47° to either a larger angle (e.g. 120°) or a smaller angle (e.g. 90°) does not have a strong effect on the LLCP, even with rigid bonds ($k_\theta = k_r = \infty$). Examination of the Si/O coordination numbers $(n_{\mathrm{Si}}, n_{\mathrm{O}})$ confirms that there is no significant change when we vary the bond angle θ_0, indicating that the overall structure of the liquid does not change when we adjust the O-Si-O bond angle. For all values of θ_0 considered, we find that the coordination numbers still approach $(n_{\mathrm{Si}}, n_{\mathrm{O}}) \to (4,4)$ at low temperatures and low densities, which implies a tetrahedral structure.

This result suggests that the liquid continues to form a tetrahedral network even when the molecules themselves do not possess tetrahedral angles. We must conclude that the tetrahedrality originates from the non-bonded terms in Eq. 1, in other words, the electrostatic interaction together with the Buckingham potential that exists between the ions. It would be interesting to see in a future study how we can disrupt the formation of the tetrahedral network and see how this affects the LLCP.

Finally, we would like to point out to the reader that in the case where the LLCP disappears below the spinodal (Fig. 5f), the modified-WAC model realizes the "critical point free" scenario. This scenario is one of many scenarios suggested as a possible explanation for the origin of the anomalies present in liquid water[82–84]. It is also possible that this scenario occurs in liquid silicon, considering that the Stillinger-Weber model for silicon is close to realizing the critical point free scenario[80]. Figs. 4 and 5 also show signs of a re-entrant spinodal, which is another scenario that was proposed for liquid water but later rejected. However, recent work[85,86] shows that a re-entrant spinodal might still be a possible scenario. Considering that our model can be used to reproduce these various scenarios, it might be interesting in future work to explore these phenomena using the bonded modified WAC model.

AUTHOR DECLARATIONS

Conflict of Interest

The author has no conflicts to disclose.

DATA AVAILABILITY

Data available on request from the author.

REFERENCES

[1] P. H. Poole, F. Sciortino, U. Essmann, and H. E. Stanley, *Nature* **360**, 324 (1992).
[2] F. H. Stillinger and A. Rahman, *J. Chem. Phys.* **60**, 1545 (1974).
[3] A. Nilsson and L. G. M. Pettersson, *Nat. Commun.* **6**, 8998 (2015).
[4] P. Gallo, K. Amann-Winkel, C. A. Angell, M. A. Anisimov, F. Caupin, C. Chakravarty, E. Lascaris, T. Loerting, A. Z. Panagiotopoulos, J. Russo, J. A. Sellberg, and H. E. Stanley, *Chem. Rev.* **116**, 7463 (2016).
[5] D. T. Limmer and D. Chandler, *J. Chem. Phys.* **135**, 134503 (2011).
[6] Y. Liu, J. C. Palmer, A. Z. Panagiotopoulos, and P. G. Debenedetti, *J. Chem. Phys.* **137**, 214505 (2012).
[7] J. C. Palmer, R. Car, and P. G. Debenedetti, *Faraday Discuss.* **167**, 77 (2013).
[8] D. T. Limmer and D. Chandler, *J. Chem. Phys.* **138**, 214504 (2013).
[9] T. A. Kesselring, E. Lascaris, G. Franzese, S. V. Buldyrev, H. J. Herrmann, and H. E. Stanley, *J. Chem. Phys.* **138**, 244506 (2013).
[10] P. H. Poole, R. K. Bowles, I. Saika-Voivod, and F. Sciortino, *J. Chem. Phys.* **138**, 034505 (2013).
[11] J. C. Palmer, F. Martelli, Y. Liu, R. Car, A. Z. Panagiotopoulos, and P. G. Debenedetti, *Nature* **510**, 385 (2014).
[12] V. Holten, J. C. Palmer, P. H. Poole, P. G. Debenedetti, and M. A. Anisimov, *J. Chem. Phys.* **140**, 104502 (2014).
[13] F. Smallenburg, P. H. Poole, and F. Sciortino, *Mol. Phys.* **113**, 2791 (2015).
[14] D. Corradini, M. Rovere, and P. Gallo, *J. Chem. Phys.* **132**, 134508 (2010).
[15] J. L. F. Abascal and C. Vega, *J. Chem. Phys.* **133**, 234502 (2010).
[16] D. Paschek, A. Rüppert, and A. Geiger, *ChemPhysChem* **9**, 2737 (2008).
[17] P. G. Debenedetti, F. Sciortino, and G. Zerze, *Science* **369**, 289 (2020).
[18] M. Yamada, S. Mossa, H. E. Stanley, and F. Sciortino, *Phys. Rev. Lett.* **88**, 195701 (2002).
[19] D. Paschek, *Phys. Rev. Lett.* **94**, 217802 (2005).
[20] N. Giovambattista, T. Loerting, B. R. Lukanov, and F. W. Starr, *Sci. Rep.* **2**, 390 (2012).
[21] E. B. Moore and V. Molinero, *Nature* **479**, 506 (2011).
[22] V. Holten, D. T. Limmer, V. Molinero, and M. A. Anisimov, *J. Chem. Phys.* **138**, 174501 (2013).
[23] E. A. Jagla, *Phys. Rev. E* **63**, 061501 (2001).
[24] G. Franzese, G. Malescio, A. Skibinsky, S. V. Buldyrev, and H. E. Stanley, *Nature* **409**, 692 (2001).
[25] G. Franzese, G. Malescio, A. Skibinsky, S. V. Buldyrev, and H. E. Stanley, *Phys. Rev. E* **66**, 051206 (2002).
[26] N. B. Wilding and J. E. Magee, *Phys. Rev. E* **66**, 031509 (2002).
[27] P. Kumar, S. V. Buldyrev, F. Sciortino, E. Zaccarelli, and H. E. Stanley, *Phys. Rev. E* **72**, 021501 (2005).
[28] L. Xu, S. V. Buldyrev, C. A. Angell, and H. E. Stanley, *Phys. Rev. E* **74**, 031108 (2006).
[29] H. M. Gibson and N. B. Wilding, *Phys. Rev. E* **73**, 061507 (2006).
[30] G. Franzese, *J. Mol. Liq.* **136**, 267 (2007).
[31] A. J. Archer and N. B. Wilding, *Phys. Rev. E* **76**, 031501 (2007).
[32] L. Xu, S. V. Buldyrev, N. Giovambattista, C. A. Angell, and H. E. Stanley, *J. Chem. Phys.* **130**, 054505 (2009).
[33] L. Xu, N. Giovambattista, S. V. Buldyrev, P. G. Debenedetti, and H. E. Stanley, *J. Chem. Phys.* **134**, 064507 (2011).
[34] P. Gallo and F. Sciortino, *Phys. Rev. Lett.* **109**, 177801 (2012).
[35] P. Gallo, F. Sciortino, P. Tartaglia, and S.-H. Chen, *Phys. Rev. Lett.* **76**, 2730 (1996).
[36] F. Sciortino, P. Gallo, P. Tartaglia, and S.-H. Chen, *Phys. Rev. E* **54**, 6331.
[37] L. M. Martinez and C. A. Angell, *Nature* **410**, 663 (2001).
[38] F. Smallenburg, L. Filion, and F. Sciortino, *Nature Phys.* **10**, 653 (2014).
[39] Y. Katayama, T. Mizutani, W. Utsumi, O. Shimomura, M. Yamakata, and K.-I. Funakoshi, *Nature* **403**, 170 (2000).
[40] Y. Katayama, *J. Non-Cryst. Solids* **312**, 8 (2002).
[41] Y. Katayama, Y. Inamura, T. Mizutani, M. Yamakata, W. Utsumi, and O. Shimomura, *Science* **306**, 848 (2004).
[42] D. Hohl and R. O. Jones, *Phys. Rev. B* **50**, 17047 (1994).
[43] L. M. Ghiringhelli and E. J. Meijer, *J. Chem. Phys.* **122**, 184510 (2005).
[44] L. M. Ghiringhelli and E. J. Meijer, *J. Phys.: Condens. Matter* **19(41)**, 416104 (2007).
[45] R. Shimizu, M. Kobayashi, and H. Tanaka, *Phys. Rev. Lett.* **112**, 125702 (2014).
[46] M. Kobayashi, R. Shimizu, and H. Tanaka, *J Phys Chem B.* **119(35)**, 11768 (2015).
[47] M. Kobayashi and H. Tanaka, *Nat. Commun.* **7**, 13438 (2016).
[48] F. Walton, J. Bolling, A. Farrell, J. MacEwen, C. D. Syme, M. G. Jiménez, H. M. Senn, C. Wilson, G. Cinque, and K. Wynne, *J. Am. Ceram. Soc.* **142, 16**, 7591 (2020).
[49] L. Henry, M. Mezouar, G. Garbarino, D. Sifré, G. Weck, and F. Datchi, *Nature* **584**, 382 (2020).
[50] L. V. Woodcock, C. A. Angell, and P. Cheeseman, *J. Chem. Phys.* **65**, 1565 (1976).
[51] E. Lascaris, M. Hemmati, S. V. Buldyrev, H. E. Stanley, and C. A. Angell, *J. Chem. Phys.* **140**, 224502 (2014).
[52] E. Lascaris, *Phys. Rev. Lett.* **116**, 125701 (2016).
[53] R. Chen, E. Lascaris, and J. C. Palmer, *J. Chem. Phys.* **146**, 234503 (2017).
[54] B. W. H. van Beest, G. J. Kramer, and R. A. van Santen, *Phys. Rev. Lett.* **64**, 1955 (1990).
[55] M. Hemmati and C. A. Angell, *J. Non-Cryst. Solids* **217**, 236 (1997).
[56] I. Saika-Voivod, F. Sciortino, and P. H. Poole, *Phys. Rev. E* **69**, 041503 (2004).
[57] P. H. Poole, M. Hemmati, and C. A. Angell, *Phys. Rev. Lett.* **79**, 2281 (1997).
[58] I. Saika-Voivod, F. Sciortino, and P. H. Poole, *Phys. Rev. E* **63**, 011202 (2000).
[59] C. A. Angell and M. Hemmati, Glass Transitions and Critical Points in Orientationally Disordered Crystals and Structural Glassformers: "Strong" Liquids are More Interesting Than We Thought, in *4th International Symposium on Slow Dynamics in Complex Systems*, edited by M. Tokuyama and I. Oppenheim, volume 1518, p. 9, AIP Conf. Proc., 2013.
[60] E. Lascaris, M. Hemmati, S. V. Buldyrev, H. E. Stanley, and C. A. Angell, *J. Chem. Phys.* **142**, 104506 (2015).
[61] F. Jensen, *Introduction to Computational Chemistry*, John Wiley & Sons, 2nd edition, 2007.
[62] S. Miyamoto and P. A. Kollman, *J. Comp. Chem.* **13**, 952 (1992).
[63] H. C. Andersen, *J. Comp. Phys.* **52**, 24 (1983).
[64] J.-P. Ryckaert, G. Ciccotti, and H. J. C. Berendsen, *J. Comp. Phys.* **23**, 327 (1977).
[65] B. Hess, C. Kutzner, D. van der Spoel, and E. Lindahl, *J. Chem. Theory Comp.* **4**, 435 (2008).
[66] This lack of support is not mentioned in the Gromacs manual. Only when one tries to run a simulation does Gromacs indicate that "the Verlet cutoff-scheme does not (yet) support the Buckingham potential".
[67] The hardware acceleration in Gromacs 4.6.7 uses the XOP instruction set, which is no longer supported by AMD computer chips.

[68]G. Bussi, D. Donadio, and M. Parrinello, *J. Chem. Phys.* **126**, 014101 (2007).
[69]OPLS/AA force field parameters can be found in the topology file `oplsaa.ff/ffbonded.itp` which is part of the Gromacs 4.6.7 package.
[70]Y. Xu, N. G. Petrik, R. S. Smith, B. D. Kay, and G. A. Kimmel, *Proc. Natl. Acad. Sci. U.S.A.* **113**, 14921 (2016).
[71]J. Q. Broughton, G. H. Gilmer, and K. A. Jackson, *Phys. Rev. Lett.* **49**, 1496 (1982).
[72]J. W. Cahn, W. B. Hillig, and G. W. Sears, *Acta Metall.* **12**, 1421 (1964).
[73]R. G. Fernández, J. L. Abascal, and C. Vega, *J. Chem. Phys.* **124**, 144506 (2006).
[74]H. Tanaka, *EPL* **50**, 340 (2000).
[75]C. E. Bertrand and M. A. Anisimov, *J. Phys. Chem. B* **115**, 14099 (2011).
[76]V. Holten and M. A. Anisimov, *Sci. Rep.* **2**, 713 (2012).
[77]H. Tanaka, *Faraday Discuss.* **167**, 9 (2013).
[78]V. Molinero, S. Sastry, and C. A. Angell, *Phys. Rev. Lett.* **97**, 075701 (2006).
[79]F. H. Stillinger and T. A. Weber, *Phys. Rev. B* **31**, 5262 (1985).
[80]V. V. Vasisht, S. Saw, and S. Sastry, *Nature Phys.* **7**, 549 (2011).
[81]F. Smallenburg and F. Sciortino, *Phys. Rev. Lett.* **115**, 015701 (2015).
[82]P. H. Poole, F. Sciortino, T. Grande, H. E. Stanley, and C. A. Angell, *Phys. Rev. Lett.* **73**, 1632 (1994).
[83]S. Sastry, P. G. Debenedetti, F. Sciortino, and H. E. Stanley, *Phys. Rev. E* **53**, 6144 (1996).
[84]C. A. Angell, *Science* **319**, 582 (2008).
[85]L. Rovigatti, V. Bianco, J. Tavares, and F. Sciortino.
[86]P. Chitnelawong, F. Sciortino, and P. H. Poole, *J. Chem. Phys.* **150**, 234502 (2019).

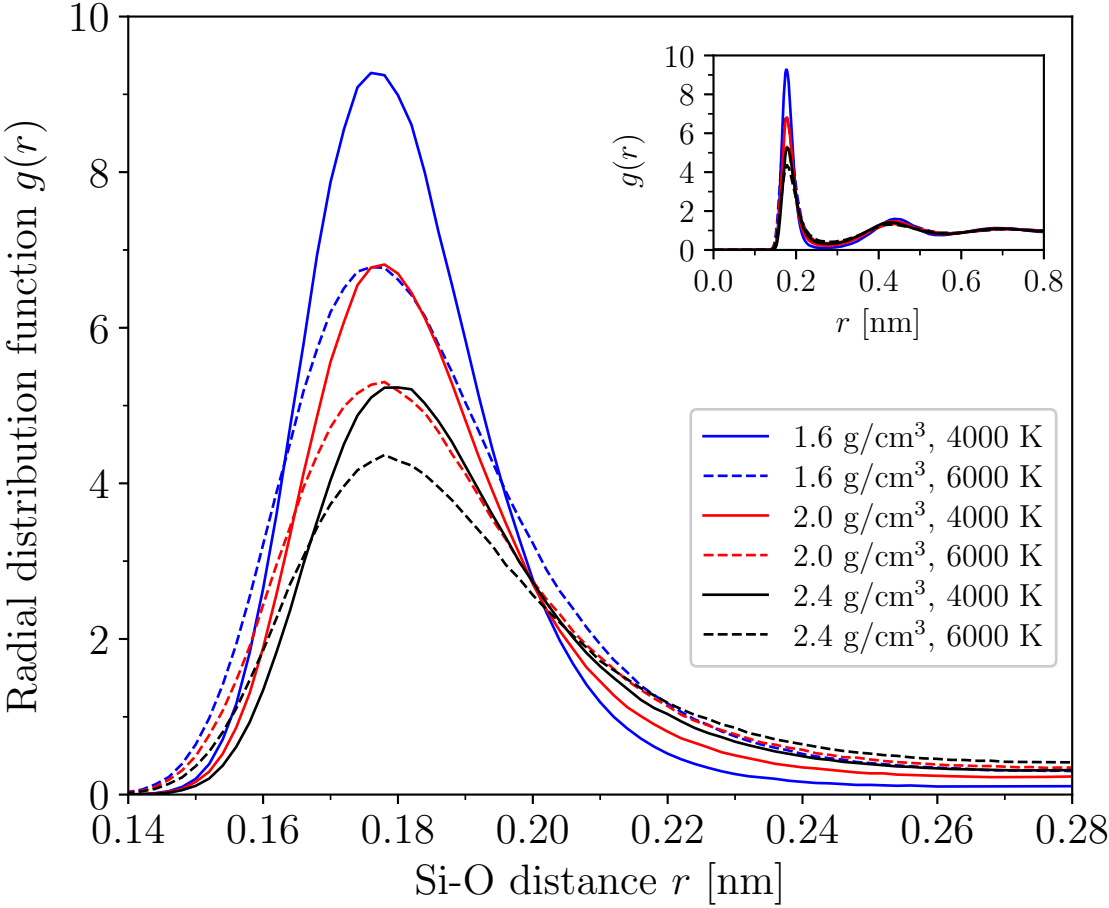
Radial distribution function $g(r)$
Si-O distance r [nm]
1.6 g/cm^3, 4000 K
1.6 g/cm^3, 6000 K
2.0 g/cm^3, 4000 K
2.0 g/cm^3, 6000 K
2.4 g/cm^3, 4000 K
2.4 g/cm^3, 6000 K
$g(r)$
r [nm]

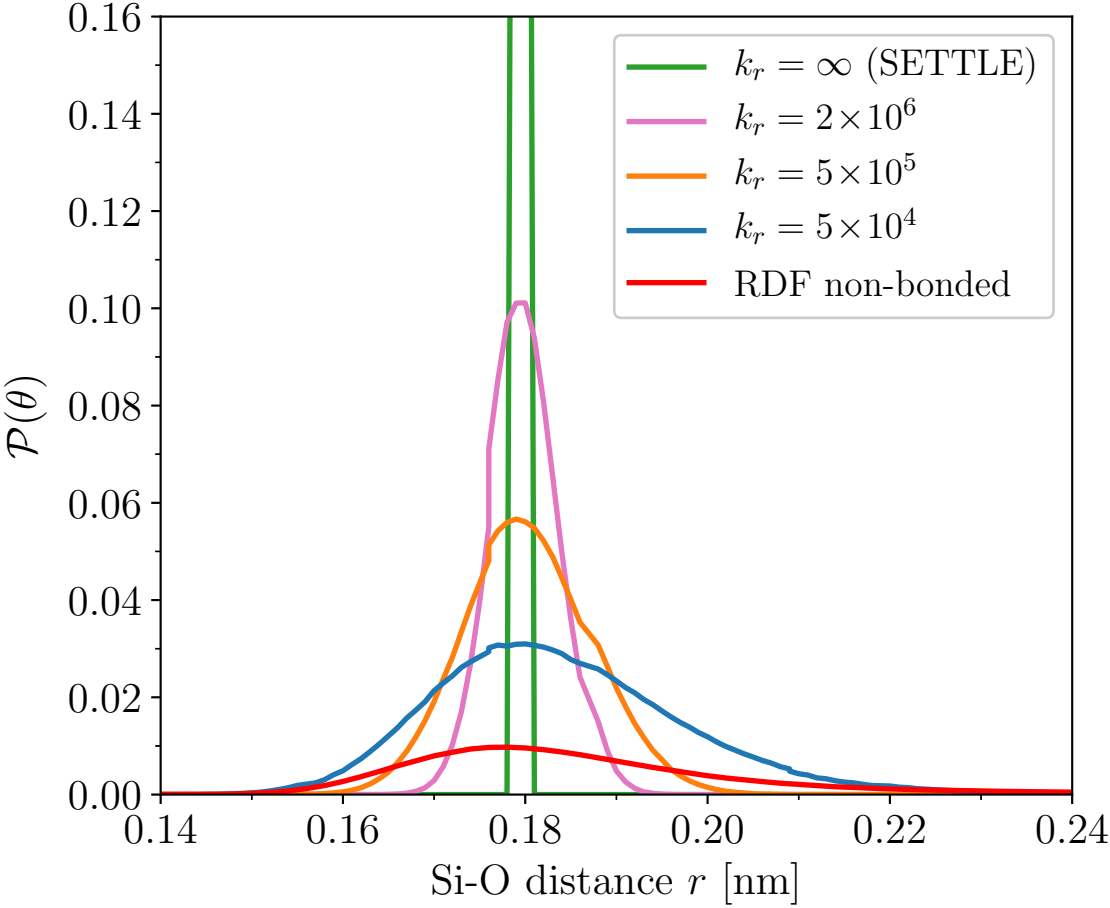
0.16
0.14
0.12
0.10
0.08
0.06
0.04
0.02
0.00
$\mathcal{P}(\theta)$
0.14
0.16
0.18
0.20
0.22
0.24
Si-O distance r [nm]
$k_r = \infty$ (SETTLE)
$k_r = 2\times10^6$
$k_r = 5\times10^5$
$k_r = 5\times10^4$
RDF non-bonded

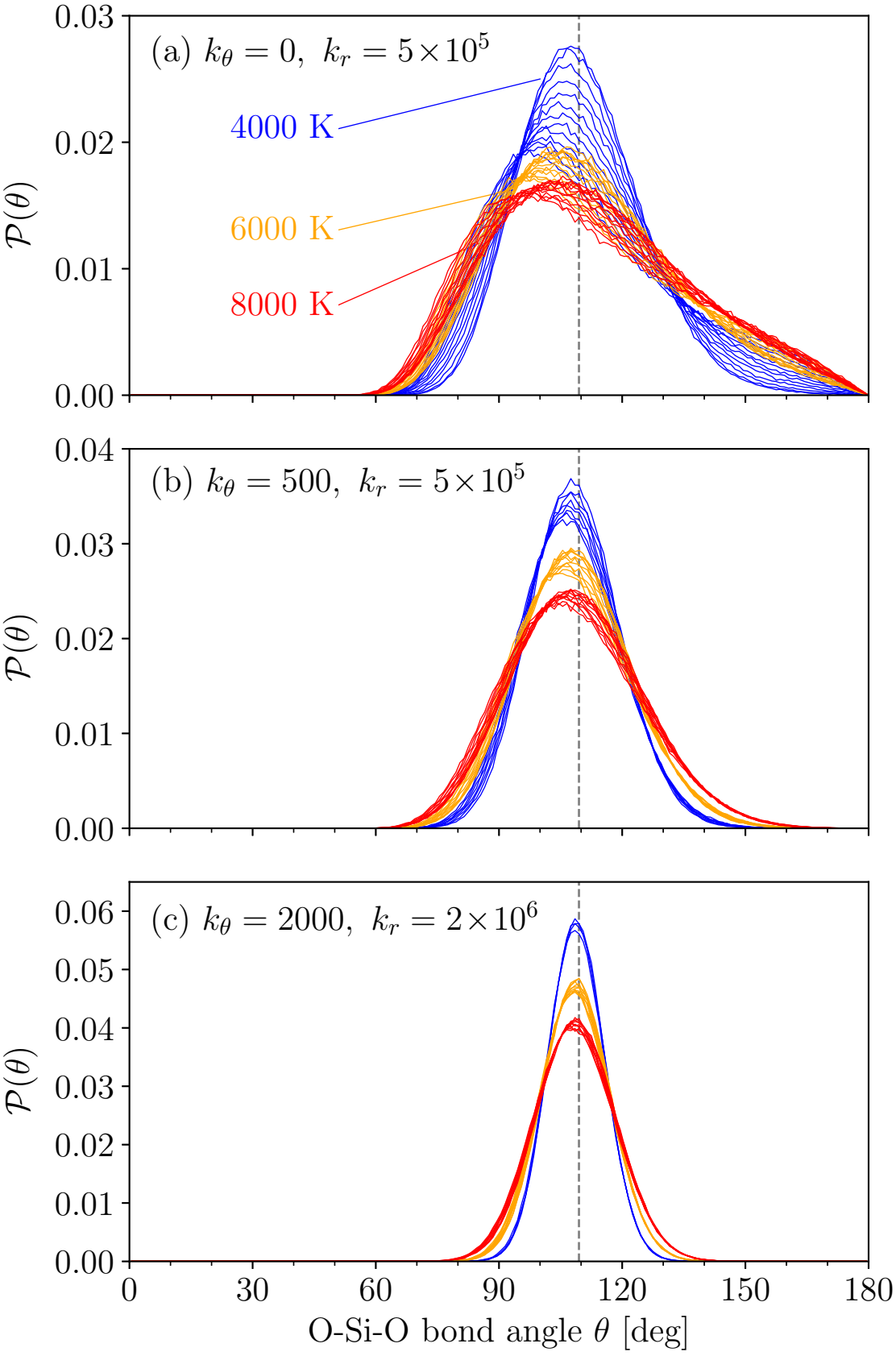
(a) $k_\theta = 0,\ k_r = 5\times10^5$
4000 K
6000 K
8000 K
(b) $k_\theta = 500,\ k_r = 5\times10^5$
(c) $k_\theta = 2000,\ k_r = 2\times10^6$
$\mathcal{P}(\theta)$
0.00
0.01
0.02
0.03
0.04
0.05
0.06
0
30
60
90
120
150
180
O-Si-O bond angle θ [deg]

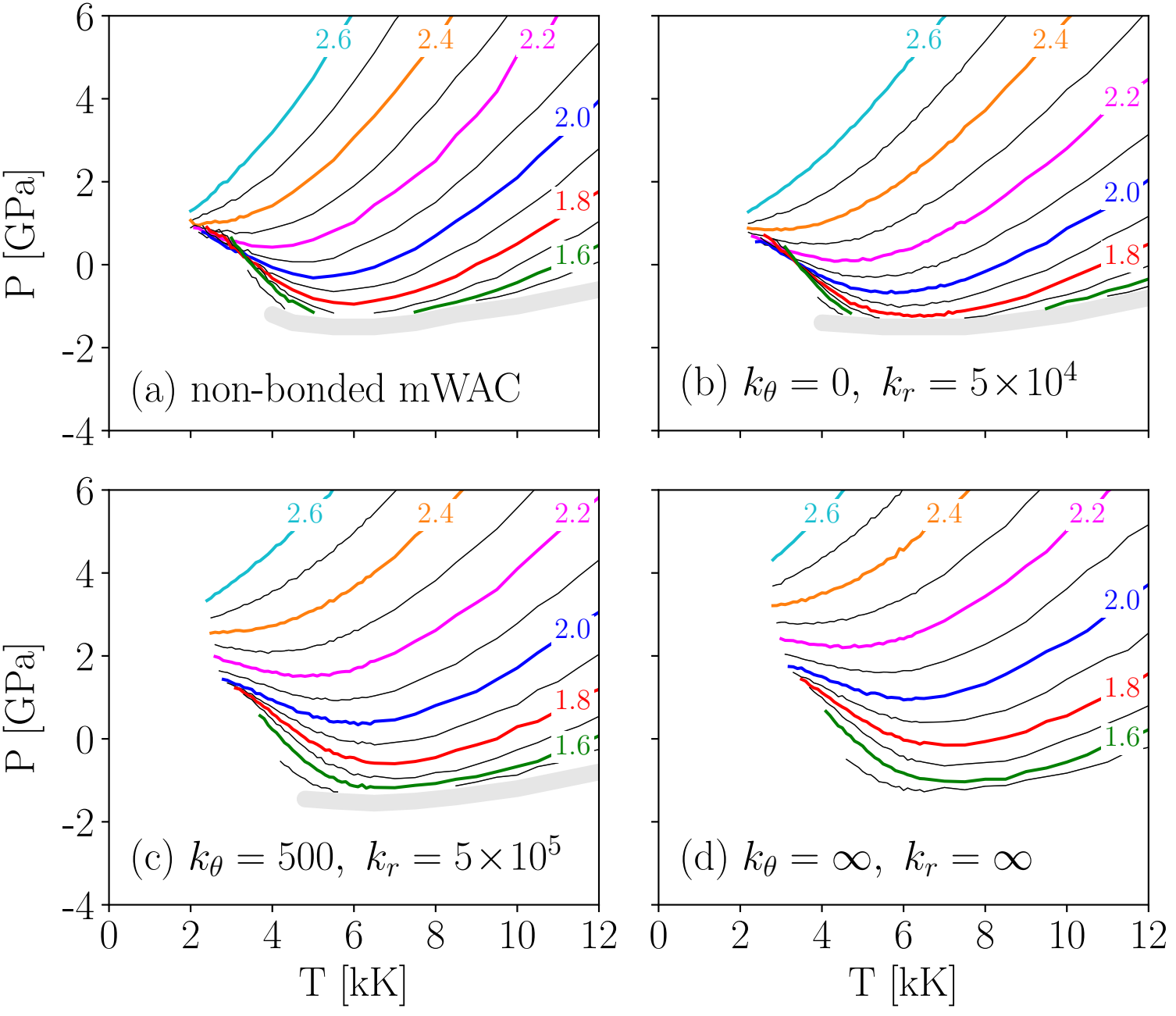
P [GPa]
T [kK]
2.6
2.4
2.2
2.0
1.8
1.6
(a) non-bonded mWAC
(b) $k_\theta = 0,\ k_r = 5\times10^4$
(c) $k_\theta = 500,\ k_r = 5\times10^5$
(d) $k_\theta = \infty,\ k_r = \infty$

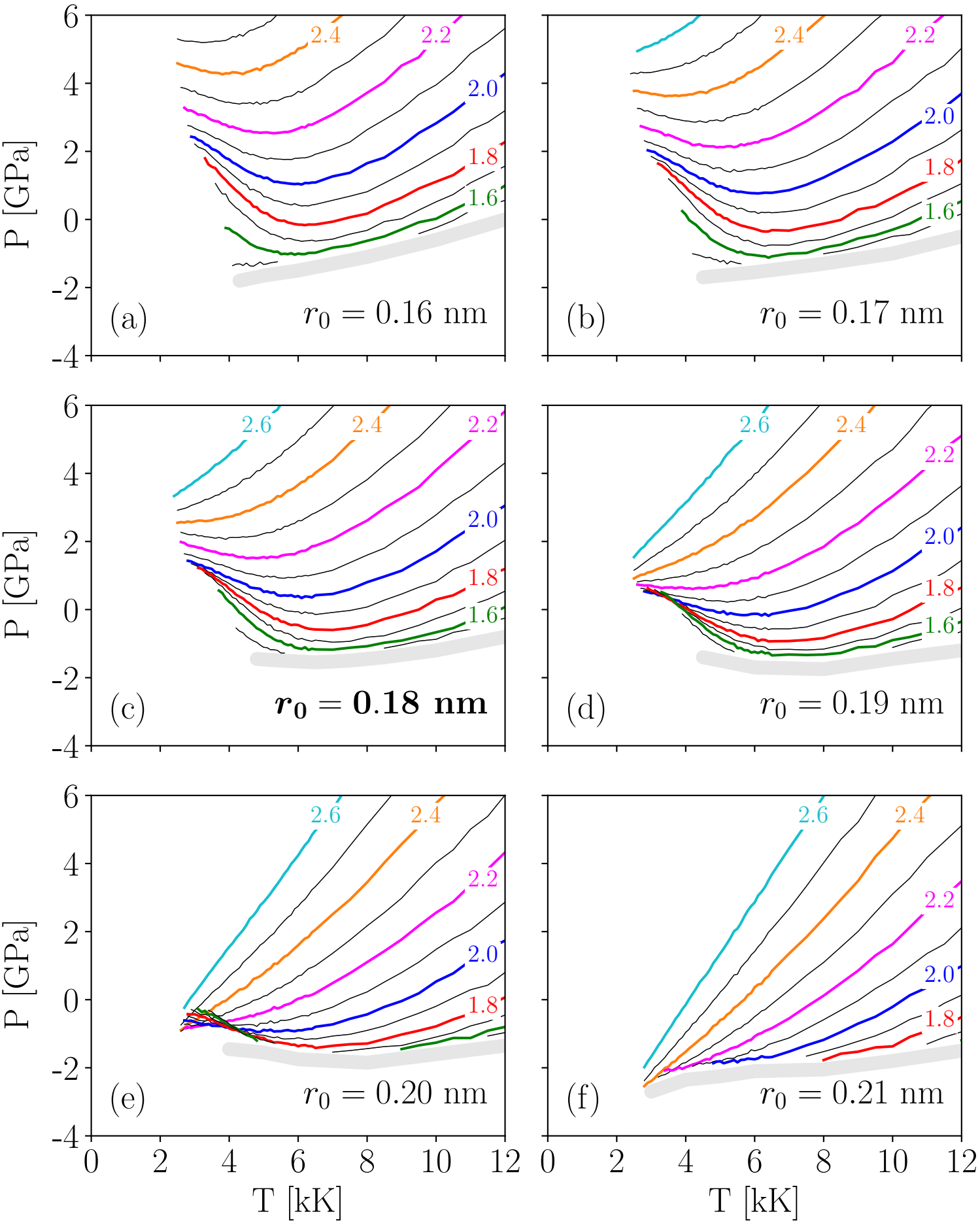
P [GPa]
T [kK]
(a)
$r_0 = 0.16$ nm
(b)
$r_0 = 0.17$ nm
(c)
$\boldsymbol{r_0 = 0.18}$ **nm**
(d)
$r_0 = 0.19$ nm
(e)
$r_0 = 0.20$ nm
(f)
$r_0 = 0.21$ nm
2.6
2.4
2.2
2.0
1.8
1.6

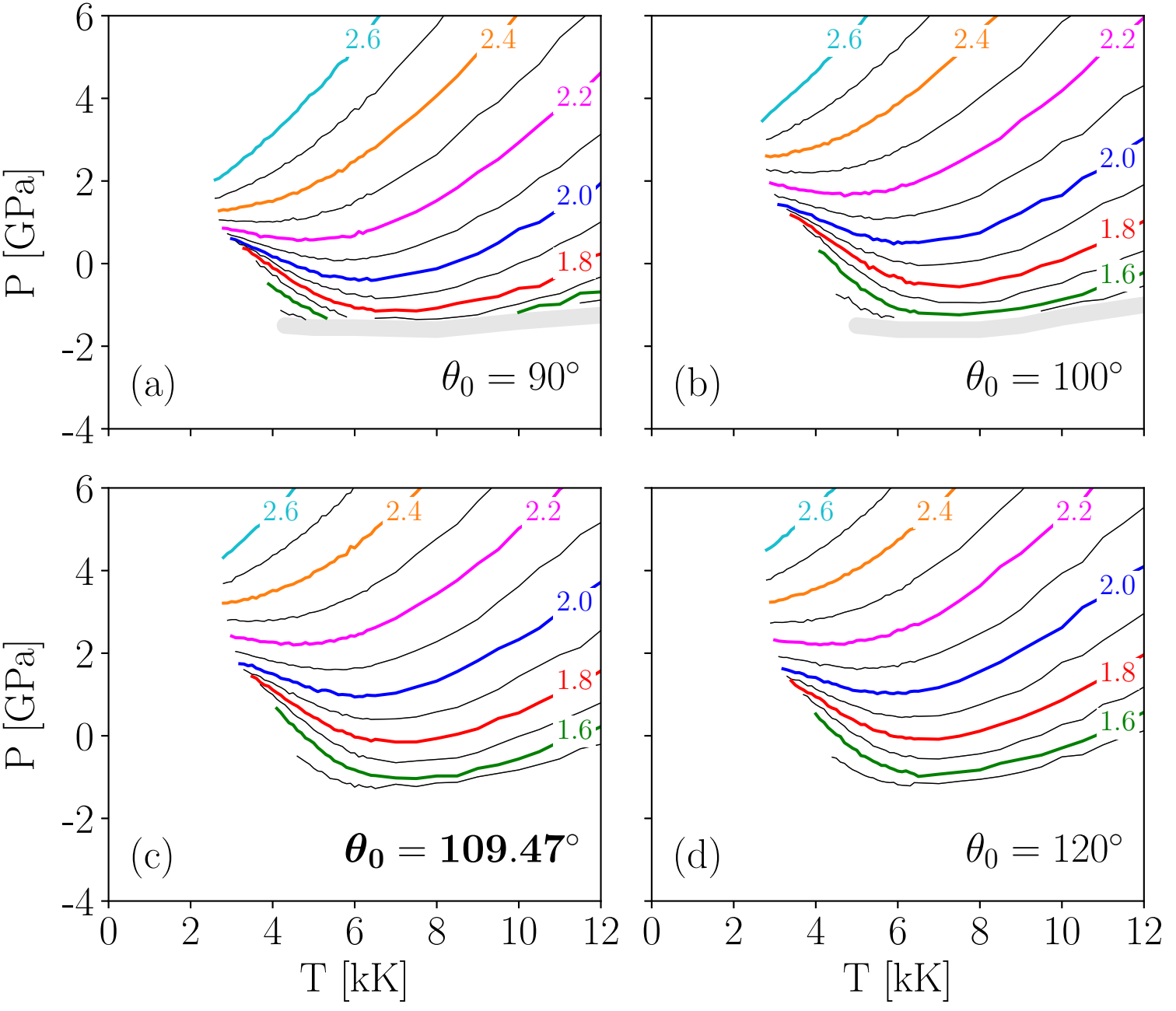
P [GPa]
T [kK]
2.6
2.4
2.2
2.0
1.8
1.6
(a)
$\theta_0 = 90°$
(b)
$\theta_0 = 100°$
(c)
$\boldsymbol{\theta_0 = 109.47°}$
(d)
$\theta_0 = 120°$

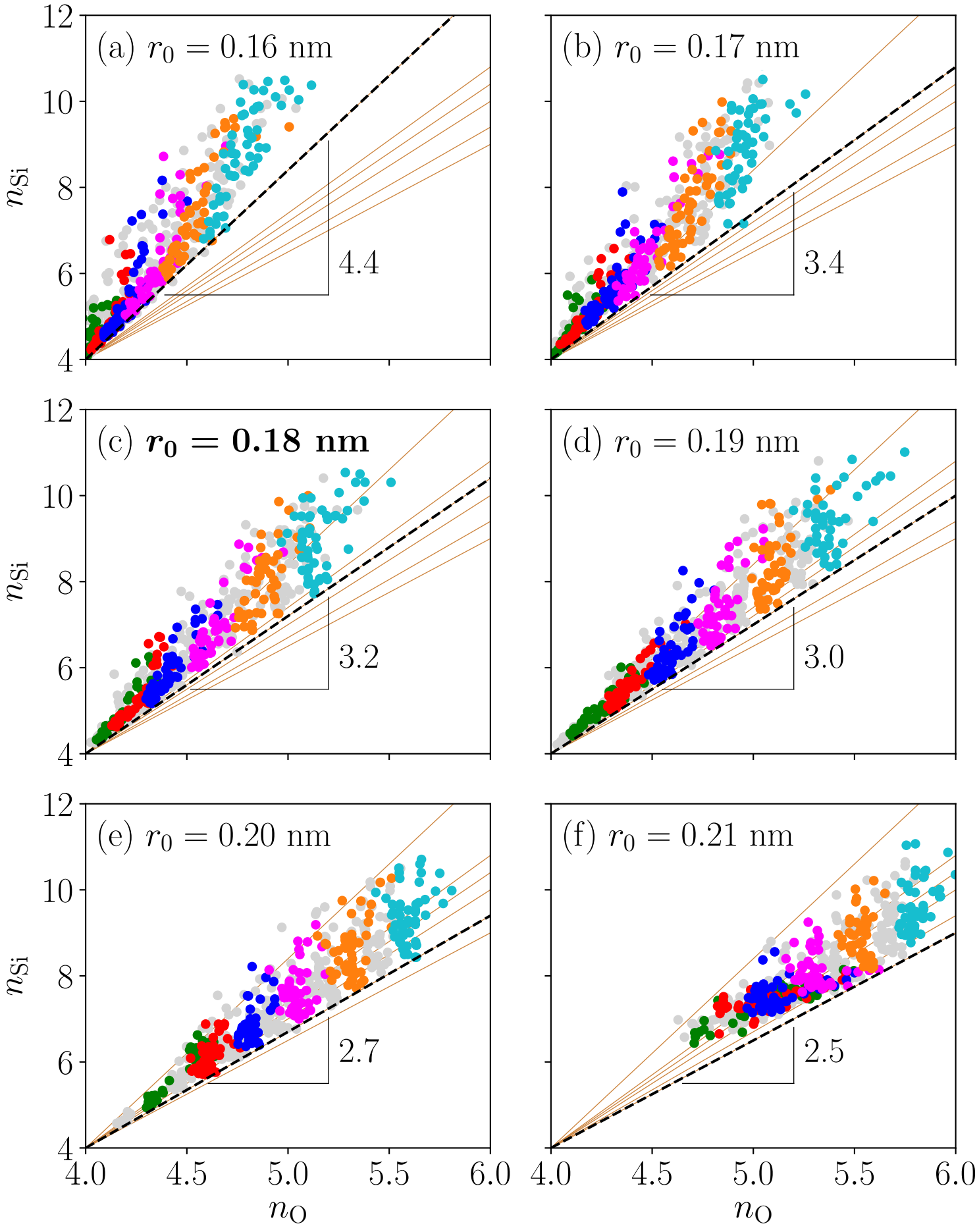
(a) $r_0 = 0.16$ nm
4.4
(b) $r_0 = 0.17$ nm
3.4
(c) $\boldsymbol{r_0 = 0.18}$ **nm**
3.2
(d) $r_0 = 0.19$ nm
3.0
(e) $r_0 = 0.20$ nm
2.7
(f) $r_0 = 0.21$ nm
2.5
n_{Si}
n_{O}
4
6
8
10
12
4.0
4.5
5.0
5.5
6.0

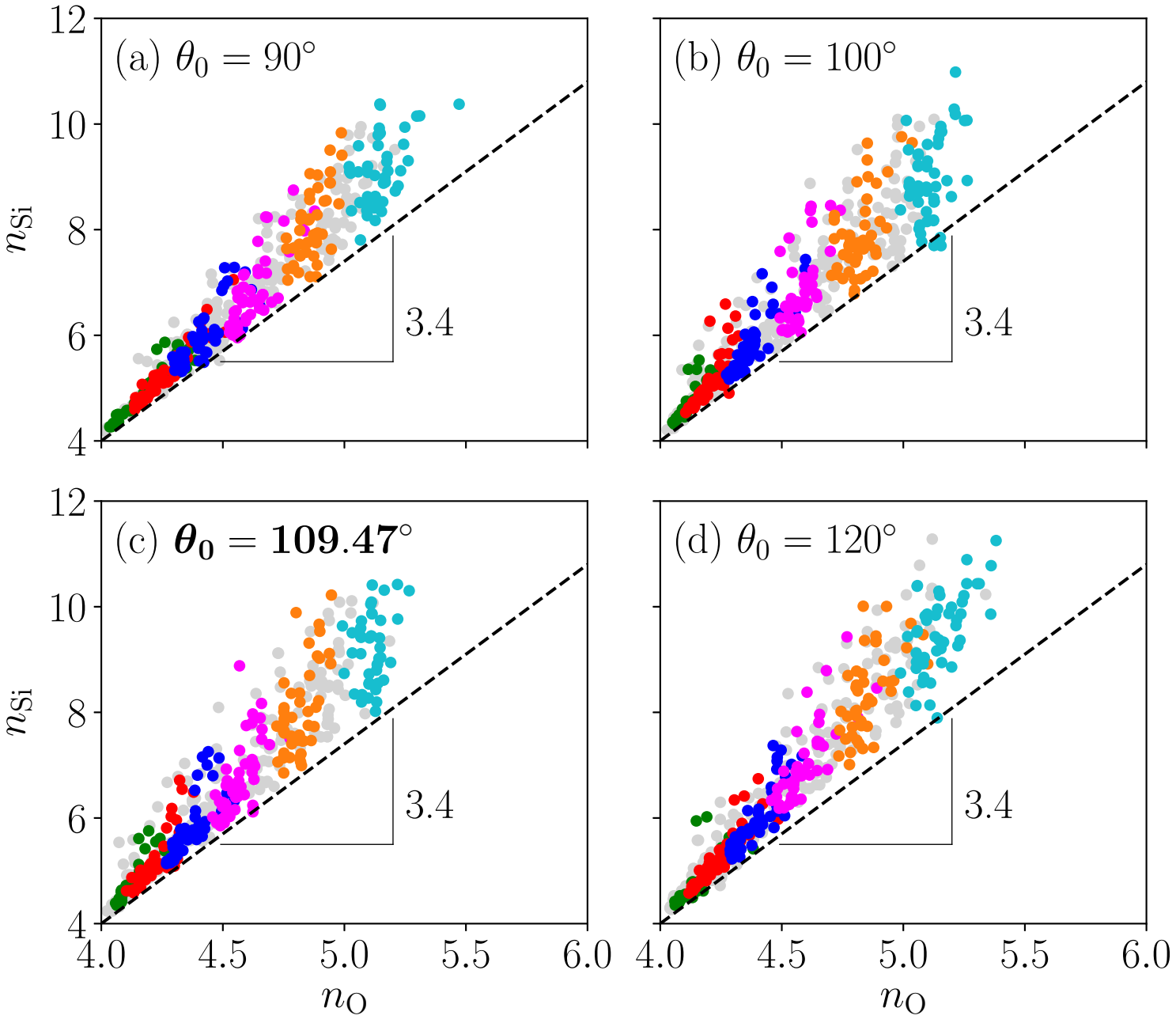
(a) $\theta_0 = 90°$
(b) $\theta_0 = 100°$
(c) $\boldsymbol{\theta_0 = 109.47°}$
(d) $\theta_0 = 120°$
3.4
n_{Si}
n_{O}
12
10
8
6
4
4.0
4.5
5.0
5.5
6.0

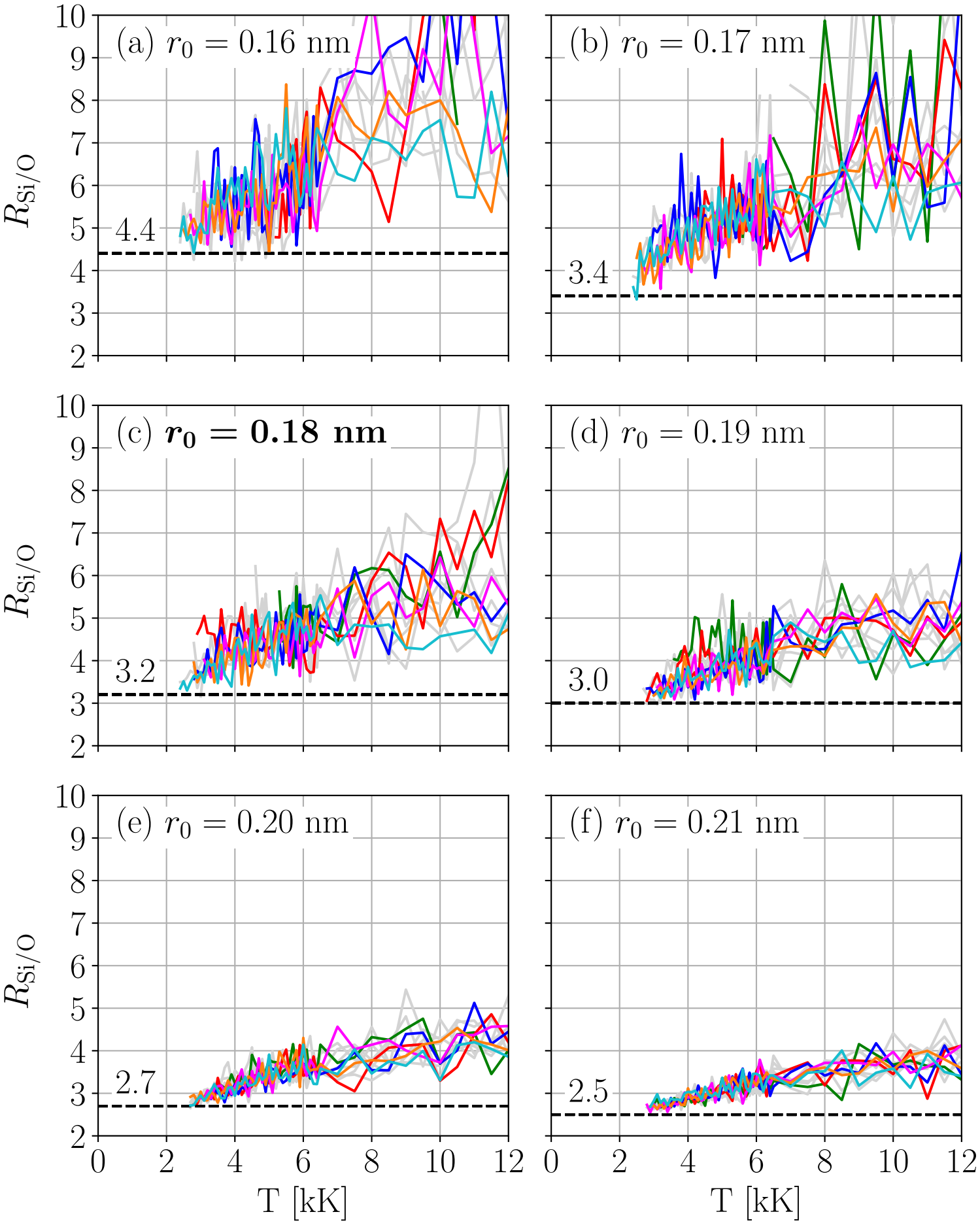
(a) $r_0 = 0.16$ nm
4.4
(b) $r_0 = 0.17$ nm
3.4
(c) $\boldsymbol{r_0 = 0.18}$ **nm**
3.2
(d) $r_0 = 0.19$ nm
3.0
(e) $r_0 = 0.20$ nm
2.7
(f) $r_0 = 0.21$ nm
2.5
$R_{\mathrm{Si/O}}$
T [kK]

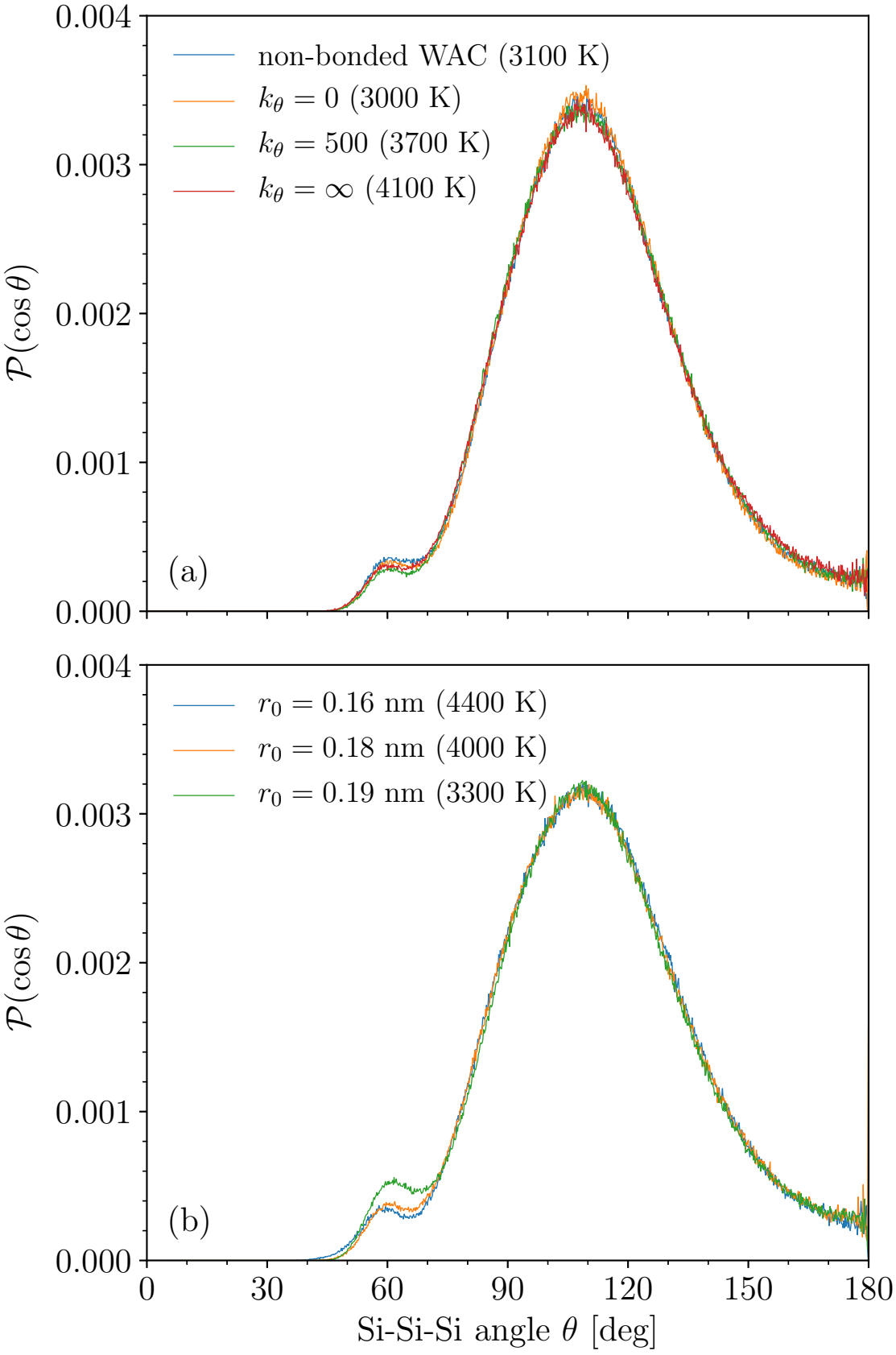
non-bonded WAC (3100 K)
$k_\theta = 0$ (3000 K)
$k_\theta = 500$ (3700 K)
$k_\theta = \infty$ (4100 K)
(a)
$r_0 = 0.16$ nm (4400 K)
$r_0 = 0.18$ nm (4000 K)
$r_0 = 0.19$ nm (3300 K)
(b)
$\mathcal{P}(\cos\theta)$
0.000
0.001
0.002
0.003
0.004
0
30
60
90
120
150
180
Si-Si-Si angle θ [deg]